

University of Alberta

**Estimating Visibility during
Snowfall Using Radar**

By

Duanni Mary Qian

A thesis submitted to the Faculty of Graduate Studies and Research in
Partial fulfillment of the requirements for the degree of

Master of Science

Department of Earth and Atmosphere Science

© Duanni Mary Qian
Fall 2012
Edmonton, Alberta

Permission is hereby granted to the University of Alberta Libraries to reproduce single copies of this thesis and to lend or sell such copies for private, scholarly or scientific research purpose only. Where the thesis is converted to, or otherwise made available in digital form, the University of Alberta will advise potential users of the thesis of these terms.

The author reserves all other publication and other rights in association with the copyright in the thesis and, except as herein before provided, neither the thesis nor any substantial portion thereof may be printed or otherwise reproduced in any material form whatsoever without the author's prior written permission.

Abstract

To estimate the visibility during snowfall, we compare hourly visibility (*Vis*) measurements with radar reflectivity factor (*Z*) measurements sampled over Edmonton International Airport during snowfall events from October 2010 to April 2011. The (*Z*, *Vis*) scatter diagrams showed that increasing *Z* was correlated with decreasing *Vis*. For a given *Z* observation, we found the probability distribution of *Vis*. The interquartile range with $Z \geq 20$ dBZ was smaller than the IQR with $Z < 20$ dBZ.

The scatter was not significantly affected by the temperature profile or the wet bulb potential temperature. Strong wind speed (≥ 15 knots) along with high reflectivity was associated low *Vis* (< 2 sm). Radar reflectivity data has valuable information for visibility, yet is not a substitute for human observations.

Acknowledgements

I am indebted to many individuals who provided encouragement and guidance to me in my journey. In particular, I would like to thank:

- Gerhard Reuter for his invaluable guidance, and his patience.
- Bruno Larochelle for inspiring me to do this project, and sharing his knowledge in the Canadian Radar meteorology.
- Dave Patrick for the time he spent on converting radar data format, and his invaluable advice in using the radar data.
- Ron Goodson for his help in retrieving the model data.
- Jack Dunnigan for coaching me to retrieve internal archived soundings.
- Anthony Liu for sharing his knowledge in decoding the radar data, and his encouragement.
- Curtis Moody for sharing his knowledge in calculating the web-bulb potential temperature.
- Xianmin Hu for his help in the MATLAB programming, and his advices and inspiring discussions on this thesis.
- Paul Joe, Faisal Boudala, George Isaac, Thanapon Piman for their remote helps in answering my questions in radar technology or about their papers.
- The management team of the CMAC-W for the financial support for tuitions, and the arrangement of my work during my education leaves.
- My colleagues for covering my shifts during my education leaves and trading my shifts during class time.
- Susan Black for her help in finding references.
- My fellow graduate students, Laura Castro-de la Guardia, Qiang Wang, Danny Brown, Clark Pennelly, and Tarana Mahzabin for their encouragement, and sharing of their research experiences.
- Zhong Yong, My sister in Christ, for her prayer and encouragement throughout this period of time.
- Finally, my husband, Paul Yang, and my son Andrew Yang for their love and understanding.

Praise the Lord for making this thesis possible.

Table of Contents

| | | |
|-----|---|----|
| 1. | Introduction | 1 |
| 1.1 | Terminal Aerodrome Forecasts and the principal visibility categories for aviation | 1 |
| 1.2 | Background theory related to visibility | 2 |
| 1.3 | Thesis objectives | 8 |
| 2. | Datasets and Method of Analysis | 11 |
| 2.1 | Visibility observations | 11 |
| 2.2 | Hourly surface observations | 13 |
| 2.3 | Six-hourly precipitation amounts | 14 |
| 2.4 | Radar dataset | 14 |
| 2.5 | Upper air soundings | 17 |
| 2.6 | Methodology | 19 |
| 3. | Visibility estimations using radar observations | 21 |
| 3.1 | Visibility – Radar reflectivity scatter plots | 21 |
| 3.2 | Probabilistic Visibility estimates based on radar reflectivity | 23 |
| 3.3 | Meteorological conditions affecting the <i>Vis-Z</i> relationship | 25 |
| 3.4 | Comparison between day time and night time observations | 28 |
| 3.5 | Spatial distribution of snow | 29 |
| 3.6 | Sensitivity of the <i>Vis-Z</i> relationship | 30 |
| 3.7 | Summary and discussion | 33 |
| 4. | Visibility and snowfall | 36 |
| 4.1 | Snow conditions from 1 October 2006 to April 30 2011 | 36 |
| 4.2 | <i>Vis-S</i> relationship for the winters 2006 to 2011 | 39 |
| 4.3 | Airmass analysis | 40 |
| 4.4 | Summary | 41 |
| 5. | Summary and conclusions | 42 |

| | | |
|-----|---|----|
| 5.1 | Conclusions and implications | 42 |
| 5.2 | Limitations and recommendations for further studies | 43 |
| | Tables | 45 |
| | Figures | 54 |
| | Bibliography | 74 |
| | Appendix A: Re-constructing the <i>Vis-S</i> relations of Richards | 77 |
| | Appendix B: Matching visibility with dBZ variables in different numbers of sample grids with different time window | 78 |

List of Tables

| Table | | Page |
|-------|--|------|
| 1.1 | Some of the <i>Vis</i> - <i>S</i> relationships in the literature (Rasmussen, 1999; Boudala, 2010; Richards, 1954, (see Appendix A)) to be tested. | 45 |
| 1.2 | Z- <i>S</i> relationships from the literature (cited by Rasmussen, 2003). Z is the reflectivity factor in dBZ; S is snowfall rate in mm hr ⁻¹ . | 45 |
| 2.1 | Data sets used in this study. YEG: Edmonton International Airport; WSE: Stony Plain Upper Air Station; <i>T</i> : Temperature; θ_w : wet-bulb potential temperature. | 46 |
| 2.2 | A small portion of Hourly meteorological observations recorded at the YEG airport from 3 Feb. 2011 to 5 Feb. 2011. The table lists Ceiling (height from the surface to the base of a layer of clouds aloft in 30's meter), <i>Vis</i> (prevailing visibility in km), wind direction (degree), wind speed (km hr ⁻¹), gust speed (km hr ⁻¹), dry bulb (dry-bulb temperature or temperature in °C), wet bulb (wet bulb temperature in °C), dew point (°C), RH (relative humidity in percentage), MSL press (mean sea level pressure in kPa), station pressure (station pressure in kPa), cloud opacity (tenth), and cloud amount (tenth). The last column lists the weather types (RW-, light rain shower; S-, light snow; single -, no weather reported). | 47 |
| 3.1 | Summary of reflectivity parameters (<i>Z</i> : the median value in the radar sample area; Min: the minimum) and some meteorological parameters (<i>Vis</i> : visibility; WS: wind speed; T_{sfc} : surface temperature; θ_w850 : θ_w at 850mb, θ_w700 : θ_w at 700mb; T850: temperature at 850mb; T700: temperature at 700mb) selected from the data used in Figure 3.1 with selection criteria: $Z \geq 20$ dBZ, and visibility > 6sm). | 48 |
| 3.2 | Summary of reflectivity factor parameters (<i>Z</i> : the median value in the radar sample area; Max: the maximum) and some meteorological parameters (ceiling: height from the surface to the base of a layer of clouds; <i>Vis</i> : visibility; WS: wind speed; T_{sfc} : surface temperature; θ_w850 : θ_w at 850mb, θ_w700 : θ_w at 700mb; T850: temperature at 850mb; T700: temperature at 700mb) selected from the data used in Figure 3.1 with the selection criteria: $Z < 13$ dBZ and <i>Vis</i> < 1sm or $Z < 10$ dBZ and <i>Vis</i> < 2sm. | 49 |

| | | |
|-----|---|----|
| 3.3 | The Reflectivity (dBZ) values at each grid pixel in the 5x5 grid sample area centered over YEG at 2011:02:27:21:00 UTC and 2010:10:25:20:00 UTC. The median value and standard deviation of the sample at 2011:02:27:21:00 UTC are 14 dBZ, and 6.7 respectively. The median value and standard deviation at 2010:10:25:20:00 UTC are 21 dBZ, and 1.5 respectively. | 50 |
| 3.4 | Table 3.4: Estimated <i>Vis</i> (unit: sm) value at each grid pixel (unit: dBZ) in a 5x5 grid sample area centered over YEG at 2011:02:27:21:00 UTC and 2010:10:25:20:00 UTC. The <i>Vis</i> - <i>Z</i> equation for the <i>Vis</i> estimation: $Vis=32.5*Z^{1.0}$, $r=-0.46$, $rmse=3.1sm$. The <i>Z</i> values are from Table 3.3. The median value and standard deviation of <i>Vis</i> of the sample at 2011:02:27:21:00 UTC are 2.9sm, and 0.6 respectively. The median value and standard deviation of <i>Vis</i> of the sample at 2011:02:27:21:00 UTC are 1.5, and 0.1 respectively. | 50 |
| 4.1 | The amount of water equivalent snowfall (WES), the number of days, the number hours with snow recorded in the weather group, the number of hours with <i>Vis</i> reported ≤ 5 sm, 3 sm, 2 sm, and 1 sm and with only snow recorded in the weather group in the winters from 2006-07 to 2010-11 at YEG. | 51 |
| 4.2 | The amount of water equivalent snowfall (WES), the number of days with snow recorded in the weather group, the number hours with snow recorded in the weather group, the number of hours with <i>Vis</i> reported ≤ 5 sm, 3 sm, 2 sm, and 1sm and with only snow recorded in the weather group in the winter months of 2010-11 at YEG. | 51 |
| A-1 | Precipitation rate values (<i>S</i>) and visibility values (<i>Vis</i>) read from the equations lines plotted on Figure 1.2. | 52 |
| A-2 | Correlation coefficients and coefficients of the best-fitting based on the data listed in Table A-1. <i>r</i> is correlation coefficient; <i>a</i> and <i>m</i> are referred to coefficients in the equation A-1. | 52 |
| B-1 | Correlation confident of <i>Vis</i> - <i>Z</i> pairs for different time windows, different dBZ variables over different radar sample sizes (3x3, 5x5, 7x7, and 9x9). <i>r</i> is the correlation coefficient; <i>SS</i> is data size. | 53 |

List of Figures

| Figure | | Page |
|--------|--|------|
| 1.1 | Visibility (statute mile) plotted against hourly snowfall (inches) for Canada (taken from Richards 1954). The solid curve gives the best fit to the data. The dashed curves show the limiting cases including 85% of the observations. | 54 |
| 2.1 | A PPI scan of Doppler radar reflectivity. The white concentric rings are 20 km apart. Data source: Environment Canada. Radar name: Carvel (WHK). Elevation angle: 00 degree. Color bar: reflectivity (dBZ) on the right and calculated precipitation rate on the left. Archived time: 2200 UTC, Nov. 14, 2011. | 55 |
| 2.2 | Examples of how to determining prevailing visibility. The center of the circle is the point of observation. In example I, Vis in the 1st quadrant is 1/4mi; Vis in the 2nd quadrant 1/2mi; Vis in the 3rd quadrant 2mi; Vis in the 4th quadrant 3/4mi. In example II, Vis in the 1st quadrant is 5mi; Vis in the 2nd quadrant 8mi; Vis in the 3rd quadrant 2mi; Vis in the 4th quadrant 10mi. (Environment Canada, 1977). | 56 |
| 2.3 | Diagram to illustrate a small portion of the radar scan over YEG. The grid centered over YEG denotes the reflectivity sample area in which the median reflectivity value is obtained. | 57 |
| 3.1 | Observed Visibility (sm) - Reflectivity (dBZ) data. The visibility is selected when only snow is in the weather group from hourly surface observation from 16 – 23 UTC at YEG. The reflectivity is the median CLOGZ PPI at the elevation angle of 0.0 degree in the sample area of 5 by 5 (near 2.5 km by 2.5 km) centered over YEG. The radar is located at WHK 50 km west of YEG. The scanning frequency of the radar reflectivity is 1 per 10 minutes. The number of data point on the figure is 1017. Both hourly surface observation and radar reflectivity data are from the winter of 2010-11. | 58 |
| 3.2 | The radar based <i>Vis</i> -snowfall relationships compared to observed visibility – reflectivity data. For the green line, radar reflectivity is converted into snowfall rate using $Z=1780S^{2.21}$ (Sekhon et al, 1970), and then visibility is calculated using $Vis=2.21S^{-1}$ (Rasmussen et al 1999). For the orange line, radar reflectivity is converted into snowfall rate using $Z=1780S^{2.21}$ (Sekhon et al, 1970), and then visibility is calculated using $\log(\sigma)=0.837+0.542\log(S)$; $Vis=3/\sigma$ (Boudala et al, 2008). The blue dots are the observation data, the same as what is shown in | 59 |

Figure 3.1.

- 3.3 Box-and-whisker plots of visibility (sm) for different reflectivity values (dBZ). Each box denotes the 25th-75th percentiles, with a red, heavy solid horizontal bar at the median value. The vertical lines (whiskers) extend to the maximum and minimum values. The reflectivity bins have a width of 4 centered at: 6, 10, 14, 18, 22, 26, 30, and 34 dBZ. The data are the same as the ones on Figure 3.1. 60
- 3.4 Box-and-whisker plots of snow reduced visibility (sm) for different reflectivity values (dBZ) with 30th, 40th, 50th, and 75th percentile curves in black, green, blue, and magenta respectively. The reflectivity groups and data are the same as ones in Figure 3.3. The data are the same as the ones on Figure 3.1. 61
- 3.5 Comparison of percentile $Vis - Z$ curves with empirical curves (same as ones in Figure 3.2) suggested by Rasmussen (1998) and Boudala (2010) (same as ones in figure 3.2), and with the $Vis - Z$ regression curves ($Vis = 32.46Z^1$, the correlation coefficient equal to 0.45044, and the root of mean squared error equal to 3.1sm, from the same data in Figure 3.1). 62
- 3.6 Visibility (sm) vs Reflectivity (dBZ) for different surface temperature ranges (a) for detailed temperature ranges, and (b) for coarse temperature ranges. The surface temperature data are from hourly surface observation data in the winter 2010-11. The data are the same as ones in Figure 3.1. 63
- 3.7 Visibility (sm) vs Reflectivity (dBZ) for different upper air temperature ranges (a) at 850 mb, and (b) at 700 mb. The data for visibility and radar reflectivity are the same as ones in Figure 3.1. The upper air temperatures are interpolated into temperature at every 10 minute from the hourly-forecast of vertical temperature made by GEMLAM at 1200 UTC daily. 64
- 3.8 Visibility (sm) vs Reflectivity (dBZ) for different θ_w ranges at the pressure level of (a) 850 mb, and (b) 700 mb. The observation data for visibility and radar reflectivity are the same as ones in Figure 3.1. The upper air θ_w values are interpolated at every 10 minute from the hourly-forecast of vertical θ_w made by GEMLAM at 1200 UTC daily. 65
- 3.9 The impact of wind on the relationship of visibility (sm) and reflectivity. (a) is Visibility (sm) v.s Reflectivity (dBZ) for different wind (kt) ranges; (b) is Visibility (sm) v.s wind speed (kt) for different reflectivity (dBZ) groups. The data are the same as ones in Figure 3.1. 66

- 3.10 Relationship between Snow-reduced visibility (unit: sm from hourly observation at YEG) and Reflectivity (unit: dBZ, observed from the WHK radar with the data collecting frequency of 1 per 10 minutes) the median value in the sample area of 2.5 km by 2.5 km centered over YEG during the winter season of 2010-11 (number of data point: 846). Red triangles denote the data observed from 16 to 23 UTC; the red line demoted the regression equation from the day data: $Vis=32.5Z^{1.0049}$, $r=-0.46$, $rmse=3.1$ sm . The blue dots denote the data observed from 00 – 15 UTC; the blue line denotes the regression equation from the night data: $Vis=50.4Z^{1.02}$, $r=-0.47$, $rmse=3.9$ sm. 67
- 3.11 Snow-reduced visibility from 16 – 23 UTC (unit: sm from hourly observation at YEG) against Reflectivity (unit: dBZ, observed from the WHK radar with the data collecting frequency of 1 per 10 minutes) the median value in the sample area of 2.5 km by 2.5 km centered over YEG during the winter season of 2010-11 (number of data point: 846). Data with none of Z values equal to -25.5 dBZ in the sample grid pixels are plotted in red triangles (29 data points). Data mixed with Z values equal to -25.5 dBZ in the sample grid pixels are plotted in blue dots. The red line denotes the $Vis - Z$ regression equation based on the data in the blue dots: $Vis=32.5Z^{1.0049}$, $r=-0.46$, $rmse=3.1$ sm. 68
- 3.12 Comparisons of different empirical relationships of Vis -radar-based snowfall rate and relationships of Z - S . (a) in green line, Vis calculated by $Vis=0.14S^{1.55}$ ($\theta_w=6$ °C) (Richards 1954) and S estimated by $Z=1780S^{2.21}$ (Sekhon et al, 1970); in orange line, Vis calculated by $Vis=0.43S^{0.88}$ ($\theta_w = 9$ °C) (Richards 1954) and S by $Z=1780S^{2.21}$ (Sekhon et al, 1970); in blue line, Vis calculated by $Vis=2.21S^{-1}$ (Rasmussen et al 1999) and S by $Z=1780S^{2.21}$ (Sekhon et al, 1970); in black line, Vis calculated by $\log(\sigma)=0.837+0.542\log(S)$ with $Vis=3/\sigma$ (Boudala et al, 2008) and S by $Z=1780S^{2.21}$ (Sekhon et al, 1970). (b) in green line, Vis calculated by $Vis=2.21S^{-1}$ (Rasmussen et al 1999) and S by $Z=1780S^{2.21}$ (Sekhon et al, 1970); in orange line, Vis is calculated by $Vis=2.21S^{-1}$ (Rasmussen et al 1999) and S by $Z=1050S^2$ Puhakka (1975) ; in blue line, Vis calculated by $Vis=2.21S^{-1}$ (Rasmussen et al 1999) and S by $Z=540S^2$ (Imai, 1960). (c) in black line, Vis is calculated by $Vis=0.14S^{1.55}$ ($\theta_w=6$ °C) (Richards 1954) and S by $Z=540S^2$ (Imai, 1960); in red line, Vis is calculated by $Vis=2.21S^{-1}$ (Rasmussen et al 1999) and S by $Z=1780S^{2.21}$ (Sekhon et al, 1970). The blue dots are the observation data, the same as what is shown in Figure 3.1. 69
- 4.1 The empirical Vis - S relationships compared to the observed Vis - S data (a) for the winter season of 2006-07, (b) for the winter 70

season of 2007-08, (c) for the winter season of 2008-09 (d) for the winter season of 2009-10, (e) for the winter season of 2010-11, and (f) for 5 winter seasons. The visibility data is from hourly observation in the winter seasons from 2006-07 to 2010-11. The precipitation rate data is from 6-hourly precipitation amount data in winter seasons from 2006-07 to 2010-11. The line in green denotes Richards, $Vis=0.43S^{0.88}$ (Vis in sm, S in mm hr⁻¹); the line in cyan denotes Rasmussen's equation, $Vis=2.21S^{-1}$ (Vis in cm, S in cm s⁻¹); the line in black denotes Boudala's equation, $\log(\sigma)=0.837+0.542\log(S)$, $Vis=3/\sigma$ (Vis in km, S in mm hr⁻¹). The red triangles denote the data observed during the day at 18 and 24 UTC with each hour reporting snow in the past 6 hour. The blue dots denote the data observed during the day at 06 and 12 UTC with each hour reporting snow in the past 6 hours.

- 4.2 θ_w (Web-bulb potential temperature in °C) and snow reduced Vis (sm) in the winter of 2010-2011 (Oct. 2010 to Spr. 2011). Left Y-axis is θ_w ; right Y-axis is visibility. The diagram shows the variability of θ_w during the snow season and θ_w values at the standard pressure levels. Solid red line is θ_w values at 500mb; Solid magenta line is θ_w values at 700mb; Solid cyan line is θ_w values at 850mb; Solid blue line is θ_w values at 925mb. 71
- 4.3 Temperature (°C) and snow reduced Vis (sm) in the winter of 2010-11 (Oct. 2010 to Spr. 2011). The left y-axis is temperature; the right y-axis is Vis (sm). The lines of red, magenta, cyan, and blue denote temperature at 500mb, 700mb, 850mb, and 925mb from stony plain soundings. The green dots are Vis values when only snow is recorded in the weather group from hourly observation data. 72
- A-1 θ_w curves should be representative of the airmass aloft ahead of the warm front. If airmass snow(circulation flurries) use the θ_w of the airmass. Assume no melting of the snow. Visibility restriction is due entirely to snow. If fog or haze is present, a reduction of as much as 20% would be required. This graph was modified by D. Day, Maritimes Weather Center. Original unknown, but probably from Richards' work. (MOIP, 2001). 73

1. Introduction

Environment Canada (EC) is responsible for providing weather forecasting for about 180 airports located in Canada (Transport Canada, 2011c). Weather conditions described in these forecasts include wind speed, wind direction, visibility, cloud amount, ceiling height, precipitation type and precipitation intensity. The safety and efficiency of air travel depends on the accuracy of these aviation meteorology forecasts (Hansen 2007). These forecasts are used for planning the fuel load for the flight (Transport Canada, 2011d). For example, if the forecast visibility at a particular airport is very low, the aircraft will be required to carry extra fuel in case a detour to another airport is needed. Accurate weather forecasts for the airports represent a saving to airlines in terms of reducing fuel burn, fewer diversions, and fewer fuel stops (Transport Canada, 2011a; NAV CANADA, 2002, p. 16).

Visibility (or more precisely *horizontal visibility*) is the “maximum distance at which an observer may see and identify an object lying close to the horizontal plane on which he is standing” (WMO, 1992). It is an important element of an aviation weather forecast. Transport Canada stipulates that commercial aircraft should have a prescribed minimum visibility range at an airport for safe landing (Transport Canada, 2011b; Transport Canada, 2011e).

Several meteorological conditions can affect horizontal visibilities, such as fog, pollution, rain, snowfall, and blowing snow or dust. Snow is one of the meteorological conditions that has the largest impact on horizontal visibility. Therefore, I will focus my research on the reduction of visibility due to snow.

1.1 Terminal Aerodrome Forecasts and the principal visibility categories for aviation

Visibility is an important element in an Aerodrome Forecast (TAF). TAF is defined as the forecaster’s best judgement of the most probable weather conditions expected to occur at an airdrome together with their most probable

time of occurrence” (Environment Canada, 1996, p. 2-1). The aerodrome forecast provides forecast for main weather conditions, transient weather conditions (Environment Canada, 1996, p. 2-16), and probably occurring weather conditions (Environment Canada, 1996, p. 2-14) during a specific period of time. TAF “is designed to meet the pre-flight and inflight requirements of flight operations within 5 nautical miles of the centre of the runway complex depending on local terrain” (Environment Canada, 1996, p. 2-1).

Visibility is expressed in units of statute miles (sm), with the following conversion: 1 statute mile = 0.87 nautical miles = 1.61 kilometer. The principal visibility categories are delineated into four major thresholds: First, there is the 6 *sm* minimum visibility requirement to satisfy the *non-alternate Instrument Flight Rule*. Second there is the 3 *sm* minimum visibility mandated for the *Visual Flight Rule*. Third, there is the *alternate limit visibility* for the aerodrome, mandated by Transport Canada. This differs from airport to airport. For the Edmonton International Airport (YEG) the alternate visibility limit is 1 *sm*. And fourth, there is the *minimum visibility for landing* which differs for each aerodrome, approved for Transport Canada. *For YEG, the minimum visibility approach (landing) limit is ½ sm* (Environment Canada, 1996, p. 2-1).

1.2 Background theory related to visibility

In this section, we introduce the concept of the *extinction coefficient* because it quantifies the visibility as perceived by human eyes. This provides an explanation of how precipitation particles in the atmosphere obscure an object seen by an observer, and it also can be used to formulate a theoretical relationship between visibility and snowfall. This discussion will be expanded to introduce equations which relate visibility with snowfall rate and also visibility with weather radar reflectivity factor.

Concerning the extinction coefficient, “most of the light that reaches our eyes comes through the process of scattering. Scattering is a physical process by which a particle in the path of an electromagnetic wave continuously extracts

energy from the incident wave and reradiates that energy in all directions. Scattering is often accompanied by absorption. The extinction is the result of scattering and absorption” (Liou, 1980, p. 6). The *extinction coefficient* (denoted by σ) is the fractional reduction of luminous flux per unit distance by scattering and absorption when light travels through a medium (Middleton, 1964, p13). Assuming there is no absorption, the extinction coefficient is given by the relation (Middleton, 1964, p29)

$$\sigma = \frac{1}{4} \sum_{i=1}^n N_i K_i \pi D_i^2 \quad (1)$$

where D_i is the diameter for particles in size class i , N_i is the particle density at i , K_i is the scattering area ratio, and n is the total number of scattering particles. The unit of the extinction coefficient is m^{-1} . For large scattering particles like liquid water fog, K_i is approximately 2. Meteorological visibility (Vis) during day time can be related approximately to extinction coefficient (σ) using the Koschmieder relation (Middleton, 1964, p. 105, cited by Rasmussen et al, 1999),

$$Vis = 3.912 / \sigma . \quad (2)$$

We note that from (1) and (2) it follows that Vis in falling snow is related to the snowflake size distribution. The snowflake size distribution is also related to the snowfall rate S .

a) Visibility–Snowfall (Vis - S) relationship

Richards (1954) was interested in estimating the snowfall rate based on observed visibility. His observations were summarized in a scatterplot of visibility (Vis) versus hourly snowfall accumulation (Figure 1.1). The data suggest that there is a Vis - S curve with a monotonic decrease of visibility with increasing snowfall.

A comprehensive study of Vis - S relationship was undertaken by Rasmussen et al. (1999). Snowflakes are irregular aggregates of crystals or smaller snowflakes. There is no easy way of measuring or describing their linear

dimension. Consequently, data on snowflake sizes are usually expressed in terms of the diameter of the equivalent water drop. Let D denote the diameter of the water drop produced by melting a snowflake and $N(D)dD$ denote the number of snowflakes per unit volume of air with melted diameters between D and $D + dD$. With this notation, the size distribution of snowflakes is assumed to be Marshall-Palmer distribution:

$$N(D) = N_0 \exp(-\Lambda D) \quad (3)$$

where Λ is the slope of the size distribution, N_0 is the vertical axis intercept, and D is the snowflake particle equivalent water droplet diameter with the unit of cm (Braham, 1990, cited by Rasmussen et al, 1999; Marshall et al, 1948, cited by Roger et al, 1996). The extinction coefficient (σ), accounting for scattering and absorption by particles in the volume, is expressed as (Rasmussen et al, 1999)

$$\sigma = \frac{2\pi N_0}{4} \int_0^{\infty} D^2 \exp(-\Lambda D) dD = \frac{\pi N_0 \Gamma(3)}{2\Lambda^3}, \quad (4)$$

where $\Gamma(3)=2!$. For the same snowflake idealized size distribution, the precipitation rate can be expressed as (Rasmussen et al, 1999):

$$S = \frac{\pi}{6} \rho \bar{V}_t N_0 \int_0^{\infty} D^3 \exp(-\Lambda D) dD = \frac{\pi \rho \bar{V}_t N_0 \Gamma(4)}{6\Lambda^4}, \quad (5)$$

where \bar{V}_t is the mean snow fall velocity (in units of cm s^{-1}), ρ is the mean snow particle density (g cm^{-3}), S is in the unit of cm .

Combining (2), (4), and (5), Vis can be expressed as;

$$Vis = \frac{3.912 \rho \bar{V}_t}{\Lambda} S^{-1}. \quad (6)$$

Equation (6) shows how visibility relates to snowfall rate.

Rasmussen et al. (1999) found that the product of snowflake density multiplied by the snow diameter is a constant: $\rho D = C$ (in units of g cm^{-2}). The

magnitude of C depends on whether the snow is dry or wet/rimed. Thus, Vis can be further re-expressed as

$$Vis = \frac{1.3C\bar{V}_t}{S}. \quad (7)$$

Their theoretical approach indicated that the visibility in snow depends on the type of snow, the air temperature, the degree of aggregation, and the degree of riming and melting. By taking 0.017 g cm^{-1} and 100 cm s^{-1} as the representative values for C and \bar{V}_t respectively for dry snow, and taking 0.072 g cm^{-1} and 200 cm s^{-1} as the representative values for C and \bar{V}_t respectively for wet snow, the Vis - S relationship can be expressed

$$\begin{aligned} Vis &= 2.21S^{-1} && \text{for dry snow (i.e. } T < 0 \text{ }^\circ\text{C)} \\ Vis &= 18.72S^{-1} && \text{for wet snow (i.e. } T \geq 0 \text{ }^\circ\text{C)} \end{aligned} \quad (8)$$

where S is in cm/s , Vis is in cm , and T is the surface temperature.

When comparing observations of Vis and S with (8), they found that the relationships were more accurate when applied to snow events with homogeneous snowflake types. When there was a broad range of snow types, the estimates based on (8) were less accurate. Furthermore, they noted that the relationships were different during nighttime.

Boudala et al. (2009) developed several formulas for estimating the extinction coefficient as a function of liquid equivalent snowfall rate and air temperature. Their work is based on the assumption that the snowflake size distribution follows the gamma size distribution ($N(D) = N_0 D^\mu \exp(-\lambda D)$). They found that Vis is mainly dependent on the snowfall rate (S) during snow expressed in (9), with relatively weaker dependence on temperature (T) expressed in (10).

$$\ln(\sigma) = 0.837 + 0.542 \ln(S), \quad (9)$$

$$\ln(\sigma) = 0.71 - 0.029T + 0.783 \ln(S + 0.04), \quad (10)$$

where σ is extinction coefficient (km^{-1}), S is snowfall rate (mm hr^{-1}) in (9) and (10).

With respect to the uncertainty of Vis for a given S in the observation, Boudala et al (2009) explained that the Vis distribution at a given S could be described well using the Inverse Gaussian probability density.

Previous research has shown that the relationship between visibility and snowfall rate depends on the snow distribution, snow type, temperature and snowfall speed. However, it is difficult (and expensive) to measure the distribution of the snowflake distribution, snow type and snowfall speed. The visibility is often parameterized, and/or the theoretical expression for Vis is simplified by using various assumptions. Table 1.1 lists Vis - S relationships used in this study (also see Appendix A).

b) Reflectivity – Snowfall (Z - S) relationship

Weather radar is able to “observe and measure precipitation quickly, accurately, and from great distances” (Rogers et al, 1996, p.184). “The radar transmitter generates short pulses of energy in the radio-frequency portion of the electromagnetic spectrum. These energy pulses are focused by the antenna into a narrow beam. They propagate outwards at essentially the speed of light. If the pulses intercept an object with different refractive characteristics from the air, a current is induced in the object which perturbs the pulse and causes some of its energy to be scattered. Part of the scattered energy will generally be directed back toward the antenna. If this backscattered component is sufficiently large, it will be detected by the receiver” (Rogers et al, 1996, p. 185). “The radar range equation expresses the relationship between the returned power and characteristics of the radar and the target” (Rogers et al, 1996, p. 187). For distributed targets such as raindrops, snowflakes, and cloud droplets, with the assumptions that the antenna gain is uniform within 3-dB (decibel) limits, that the beam pattern is a Gaussian beam pattern, and that the size of the precipitation is very small compared to the

radio-wave length and suitable for the application of the Rayleigh scattering law, the radar equation can be expressed (Rogers et al, 1996, p. 190):

$$\overline{P}_r = \frac{\pi^3 c}{1024 \ln 2} \underbrace{\left[\frac{P_t \tau G^2 \theta^2}{\lambda^2} \right]}_{\text{RADAR}} \underbrace{\left[|K|^2 \frac{Z}{r^2} \right]}_{\text{TARGET}}, \quad (11)$$

where \overline{P}_r is the returning power, P_t is the peak power transmitted, τ is the pulse duration, c is the light velocity, G is a dimensionless number called antenna axial gain, θ is the beam width, λ is the wavelength, K is the complex index of refraction of a sphere, r is the range, and Z is the reflectivity factor, measured in $\text{mm}^6 \text{m}^{-3}$. The radar reflectivity factor can be expressed by (Rogers et al, 1996, p. 190):

$$Z = \int_0^\infty N(D) D^6 dD. \quad (12)$$

The logarithmic version of Z , $10 \log Z$ in dBZ (decibel), is defined because the wide range of Z and P_r .

For the Marshall-Palmer distribution (3) of raindrops or snowflakes (Rogers et al, 1996, p. 191)

$$Z = N_0 \frac{6!}{\Lambda^7}. \quad (13)$$

Combining (5) with(13), the relationship between Z and S (snowfall rate, unit: mm hr^{-1}), Z can be expressed as

$$Z = \frac{6!}{\pi \rho V_t \Lambda^3} S. \quad (14)$$

Many empirical Z - S relationships were developed in past. Table 1.2 lists some of those Z - S relationships cited by Rasmussen (2003), which are used in this study.

c) Visibility - Reflectivity (*Vis*-*Z*) relationship

As discussed in (a) and (b), both *Vis* and *Z* are impacted by the slope Λ in the size distribution of snowflakes. For the same distribution, by combining equations (2), (4), and (13), the *Vis*-*Z* relationship can be expressed as:

$$Vis = \frac{896.56}{\Lambda^4} Z^{-1}. \quad (15)$$

The equation indicates that the relationship between *Vis* and radar reflectivity is also impacted by Λ .

Muench et al (1977) suggested

$$\sigma = 0.091Z^{0.41} \quad (16)$$

where *Z* is the reflectivity factor and σ is in km^{-1} .

Boudala et al (2009) developed the theoretical relationship between radar reflectivity and extinction coefficient in equation (17):

$$Z = \left(\frac{6}{\pi\rho_i}\right)^2 g^2 \frac{\Gamma(2f + \mu + 1)\lambda^{b-d-f}}{2a\Gamma(b + \mu + 1)} \sigma, \quad (17)$$

where μ is the dispersion parameter; *a*, *b*, *f*, and *g* are constants associated with particle shape; ρ_i is the density of solid ice. Boudala et al (2009) pointed out again that the relationship between visibility and reflectivity depends on the size distribution of precipitation particles.

1.3 Thesis objectives

Weather radar observations have advantages over precipitation gauge measurements in the high frequency of observation and large spatial coverage of precipitation measurements. Furthermore they provide the instantaneous precipitation rate (i.e. a snowfall rate in cm hr^{-1}) whereas rain gauge data usually only provide an accumulation of precipitation (i.e. accumulated snowfall in cm). Clearly, *visibility* by its nature is a meteorological variable that may change

rapidly in time for a given location. For example, the visibility can change from 15 sm to 1 sm or less within about 10 minutes or so. Also, a Canadian airport records a major change in visibility whenever it occurs, which differs greatly from measurements of snowfall amounts which are recorded operationally only every 6 hours. The difference in the frequency of measuring visibility and snowfall makes it problematic to correlate the *Vis* and *S* values. In contrast, radar observations of snowfall rates are operationally available every 10 minutes for all locations within the radar domain. Clearly, it makes more sense to correlate *Vis* and *Z* values.

The main objective of this thesis is to explore whether radar data can be used to estimate visibility at the runways of the Edmonton International Airport (YEG) in an operational setting. I will examine to what extent the published *Vis*-*Z* relationships are applicable to estimate the visibility. How good are these estimates? What atmospheric conditions affect the sensitivity of visibility estimates? Since the decision making of the aviation industry is often based on the probabilistic forecasts, we will investigate whether we can derive useful stochastic estimates of visibility.

The general purpose of this research is to develop visibility forecast methods that are useful for aviation forecasting during snow events at the Edmonton International Airport. The specific objectives of our research will be using operational weather radar and observation:

- To develop a method of estimating the probability distribution of visibility based on the reflectivity from a weather radar, in addition to establishing a direct relationship between visibility at the surface and reflectivity observed from a weather radar.
- To quantitatively analyse factors, such as surface temperature, upper air temperature and wet-bulb potential temperature, and snow

uniformity, and observation time which may potentially impact the visibility-reflectivity relationship

- To test the accuracy of the empirical relationships between visibility and radar based snowfall rate as estimated by weather radar using the Richards method, the Rasmussen method, and the Boudala method.

The outline for the subsequent chapters is as follows: in Chapter 2 we will describe the dataset and the methodology. We will explore the relationship between visibility and reflectivity in Chapter 3. In Chapter 4, we will investigate the relationship between visibility and snowfall in five winters from 2006-07 to 2010-11. Finally, we will conclude the study in chapter 5 with a summary of findings and recommendations.

2. Datasets and Method of Analysis

This study is based on several observational data sets for radar reflectivity, visibility, temperature, wind speed, weather type, and snowfall (Table 2.1). The radar reflectivity data used in this study were measured by Carvel radar (WHK, 53.56°N, 114.14°W), which is located about 50 km northwest of the Edmonton International Airport (YEG, 53.3°N, 113.5°W). Carvel radar data are recorded every 10 minutes. Visibility, temperature, wind speed, and weather types were all recorded hourly as part of the surface observations at YEG (Nav Canada, 2011, p. B254). 6-hourly accumulated precipitation amounts were sampled every 6 hours. Vertical profiles of temperature and humidity were recorded from synoptic balloon soundings released from Stony Plain station (WSE) at 0000 UTC and 1200 UTC. These were supplemented with model soundings from the Global Environmental Multiscale Model – Limited Area Version. The locations of YEG, WSE, and WHK are shown in Figure 2.1.

In the rest of this section, a brief introduction to visibility observations will be followed by the description of each dataset used in this research. Then, the methodology of analysis will be introduced.

2.1 Visibility observations

Visibility, in the observational context, is defined as “the greatest distance at which an object of suitable dimensions can be seen and identified” (MANOBS) (Environment Canada, 1977). It is estimated at eye level 1.8 metres above the ground with the unit of statute mile (sm) by referencing a Visibility Chart at the weather observation station. A Visibility Chart is a map which plots in degrees of azimuth and in distances (statute miles) visibility markers such as buildings, or chimneys, which surround a weather station. The value of visibility in one direction is determined by how visible the visibility marker in that direction is. Since values of visibility in different directions are often different, the horizontal circle centered at the observer is divided in to many sectors. The visibility in the

observation record is the prevailing horizontal visibility, defined as the maximum visibility common to sectors comprising one-half or more of the horizontal circle (Environment Canada, 1977). Figure 2.2 gives two examples how the prevailing visibility is determined. In example I, the prevailing visibility is $\frac{3}{4}$ sm because $\frac{3}{4}$ sm is common to 3rd quadrant and 4th quadrant. In example II, 5 sm is the prevailing visibility because 5 sm covers 270° while 8 sm only covers less than 180°.

Due to lack of sunlight during the night, visibility at night is determined with the aid of markers in the form of lights. Very powerful or focussed lights would result in a high value for the visibility, which normally would be avoided. However, obstruction lights on towers and buildings and various marker lights around an airport may be used for visibility markers. At night, in the absence of visibility makers, the visibility may be estimated by studying the appearance of a ceiling projector beam. Under conditions of good visibility, the light source is visible, but the beam is not. As the visibility deteriorates, the projector beam begins to show and becomes increasingly evident as visibility decreases. When the visibility becomes quite low, the beam takes on a diffuse appearance, and the projector itself becomes blurred. Under conditions of very low visibility, beam and projector disappear completely. With practice, the observer will find the visibility may be judged with reasonable accuracy in this way. (Environment Canada, 1977, p. 2-1 to 2-4)

The reportable values of visibility are defined as follows (Environment Canada, 1977, p. 10-13 to 10-14): When the prevailing visibility is less than 1 sm, the reportable shall be 0, $\frac{1}{8}$, $\frac{1}{4}$, $\frac{3}{8}$, $\frac{1}{2}$, and $\frac{3}{4}$ sm. For visibilities between 1 and 3 sm, the reportable values are 1, $1\frac{1}{4}$, $1\frac{1}{2}$, $1\frac{3}{4}$, 2, $2\frac{1}{4}$, $2\frac{1}{2}$, $2\frac{3}{4}$ and 3 sm. Once the visibility exceeds 3 sm, the reportable values are natural numbers with 15 sm being the maximum.

2.2 Hourly surface observations

Hourly observations are designed primarily to meet the requirements of flight personnel and other users, taken each hour on the hour when the observation time is recorded in the observation record. Most elements are observed within 10 minutes before the observation hour, except for the pressure reading which has to be done exactly on the hour (Environment Canada, 1977, p. 9-1).

The observation of wind records the average direction and speed during the two minute period ending at the time of observation at a height of 10 meter, with the unit in knots (one knot (kt) is one nautical mile per hour) (Environment Canada, 1977, p. 7-2; Transport Canada, 2011c).

Weather phenomena include all types of precipitation (such as snow, rain, freezing rain), obstruction to vision (such as fog, freezing fog), and others (such as dust, and sand storms). Occurrences of all weather phenomena and their intensity are recorded in symbols. If different types of precipitation are combined in one group, the predominant type as determined by intensity shall be reported as first. The intensity qualifier selected represents the overall intensity of the entire group. When more than one weather phenomenon is observed, each weather phenomenon shall be reported in a separated weather group in the order of precipitation, obscuration to vision, and other (Environment Canada, 1977, p. 20-10 to 20-13).

With respect to visibility, wind speed, and weather type, special weather reports (SPECIs) will be taken and sent when prevailing visibility decreases to less than, or increases to equal or exceeding, 3 sm, 1½ sm, 1 sm, ¾ sm, and ¼ sm. SPECIs are also taken when wind speed (2 min mean) increases suddenly to at least double the previously reported value and exceeds 30 knots, and when precipitation occurs or stops, or the precipitation type changes (EC, 1977, p. 10-35 to 10-37; Transport Canada, 2011c). The time signed to a record for SPECI is the time of the observation made.

Table 2.2 is an example of archived hourly observations. Each record contains the time that data was observed according to the observing time discussed above. In addition to visibility (*Vis*), wind speed (Wind Speed), temperature (Dry Bulb), weather types (Weather), many other elements are included in the hourly record. Weather types are coded. In this example, “RW-” is light rain shower, “S-” is light snow, a single “-” indicates no weather. There are also several SPECIs, noted by an “S” followed immediately after the observation time. The special report at 23:18Z 2011/02/03 was sent because it started snowing. Another special report at 16:27Z 2011/02/03 was sent due to *Vis* dropping to below 2 ½ sm from 12 sm. Historic surface observations can be retrieved from http://grp.ontario.int.ec.gc.ca/Intranet/climate/grp/criteria_selection_e.cfm?grp=108.

2.3 Six-hourly precipitation amounts

The measurement of precipitation amount is expressed in terms of six-hourly accumulated depth of water (or water equivalent in the case of snow) recorded at 00Z, 06Z, 12Z, and 18Z. In Canada, precipitation amounts are recorded in mm with an accuracy of 0.2 mm. The six-hourly snowfall amount is measured by a human with a ruler measuring the depth of new snow in several places. The unit of snowfall is centimeter. The water equivalent of the snowfall is obtained by measuring the water melted from the snow collected in the snow gauge. In Canada, one centimeter of snowfall is approximately equal to 1 millimetre of water equivalent of precipitation (Environment Canada, 1977, p. 3-9).

2.4 Radar dataset

The Carvel radar operates at a wavelength of 5.34 cm. The transmitted pulses have a peak power of 260 kW (Reuter et al, 1996). The radar collects both conventional data (reflectivity) and Doppler data (velocity, spectral width)

sampled over 10 minutes. Doppler radar reflectivity data at 0° of scanning elevation angle (the lowest elevation angle for the Carvel radar) are used in this study. The corresponding radar display for such data is the PPI display – the Plan Position Indicator representing a “horizontal view of the weather echoes or reflectivity at a single selected elevation angle. The META data files were provided by the internal archive system of the National Laboratory for Hydrometeorology and Arctic Meteorology.

The radar antenna focuses and emits energy in a microwave beam (called a pulse) like a searchlight beam at a specific azimuth (theta), and a specific elevation angle. The beam intercepted by a precipitation target is refracted. Some of the energy from the beam is backscattered into the antenna. The receiver within the antenna collects this energy. Software expresses or transforms this energy to the reflectivity factor Z in unit of $\text{mm}^6 \text{m}^{-3}$, usually expressed in dBZ (Z (in dBZ) = $10 \log Z$). Any precipitation particles, such as water, ice, or snow will refract the transmitted pulse. The distance (or range) from the antenna to precipitation target can be calculated by the speed of light and the time difference between emitting and receiving. As the radar rotates and scans through all azimuth angles, one elevation angle by one elevation angle, the desired spatial reflectivity data (Volume Scan) can be gathered. The nominal times of the scan are 0, 10, 20, 30, 40, and 50 minutes of each hour. The conventional scan is completed in the 5 minutes before the nominal time, and Doppler scans are performed in 5 minutes after the nominal time (Environment Canada, 2010; Crozier, 1986).

Z can be determined over a number of pulse volumes by sending pulses of energy at a Pulse Repetition Frequency. A pulse volume is a frustum that is bounded by the radar range resolution and radar beam width. To improve the accuracy of the Z , a number of pulse volume measurements are integrated in space to determine an average value. The spatial volumes over which samples are averaged are referred to as range bins. For the Doppler radar, data sets are collected each 0.5 degrees of azimuth, at alternate Pulse Repetition Frequency for each 0.5 km range bin (Crozier, 1986).

The Doppler component of the Carvel radar allows the radar system to measure the phase changes between transmitted and received signals, in addition to measuring the reflectivity from the target. The phase changes can be used to determine the radial velocity of the target, called the Doppler radial velocity. Doppler radial velocity, in turn, can be used to distinguish precipitation particles and ground target since precipitation particles are moving targets while any ground targets (such as hills, and poles) are stationary. This feature of Doppler radar is used to remove the noise from the ground target in the returning signals. The reflectivity data after removing the ground noise is called “collected LogZ” values (CLOGZ) (Crozier, 1986, p G-59).

In summary, the CLOGZ data from the radar scan at the lowest elevation angle capture the reflectivity caused mainly by precipitation particles since the reflectivity from stationary targets has been removed. The range bin resolution is 0.5 km; the azimuthal resolution is 0.5 degree. The temporal resolution of the data is every 10 minute. The data, collected from the radar scan at the lowest level, are assumed to most closely represent the snow at the ground.

The radar data was re-produced from the archived volumetric raw data of the radar system by the Unified Radar Processor (URP) and was stored in META data format, this data format is a mixture of ASCII header and a data section. The ASCII header contains information describing the data and data type. The data section contains reflectivity data in binary (Mahidjiba et al., 2007).

The reflectivity data were stored in one byte unsigned values (N) in the META file (IRIS, 2006, p. 3-36). An N value equal to zero means no data available. N values can be converted to the reflectivity factor in dBZ for rain, using $Z = (N - 64) / 2$ (Vaisala, 2012). Z is equal to -32 dBZ when N is equal to zero. For snow, an N value is converted to equivalent reflectivity in dBZ using $Z = (N - 64) / 2 + 6.5$ (Smith, 1984; Sauvageot, 1992, p. 113). Z is equal to -25.5 when N is equal to zero.

The radar data was provided by the National Laboratory for Hydro-meteorological and Arctic Meteorology. It took an expert in the Canadian radar system to regenerate the META data of the Carvel radar used in this study. It took about 24 hours of computing time to regenerate 2-weeks META data, and about two weeks' time for 7 months of radar data.

2.5 Upper air soundings

Upper air soundings sample vertical profiles of thermodynamic and wind data. From the temperature, pressure, and humidity profiles we can calculate the wet-bulb potential temperature values (θ_w) at different pressure levels using temperature, dewpoint, and pressure. The θ_w is obtained by lifting an air parcel adiabatically to its saturation level and then following a moist-adiabatic to the reference pressure of 1000 mb (Iribarne et al, 1981, p. 151-152). The θ_w is conservative when an air mass is lifted or descends provided there is no mixing or radiative heating. θ_w is widely used to characterize an air mass. As the air mass characteristics can affect the amount and type of snowfall. This may lead to have an impact on the visibility –snowfall (*Vis-S*) relationship. In this study we will examine the dependence on θ_w using both observed and GEMLAM -model soundings.

The observed upper air soundings were launched from Stony Plain at 0000 UTC and 1200 UTC. The θ_w and temperature are given at the standard pressure levels of 925mb, 850mb, 700mb, and 500mb. These variables will be used to give a general view of θ_w values during the snow season from October 2010 to April 2011. In addition to the observed soundings, we also use hourly model profiles of temperature and humidity predicted by the GEMLAM. These model soundings were obtained from the internal archive system of the National Laboratory for Hydrometeorology and Arctic Meteorology (HAL) located in Edmonton.

The standard pressure levels with associated meteorological elements were not always included in the model output. Therefore, the value nearest to the

standard pressure levels will be used when the standard pressure levels along with associated meteorological elements are missed in the data. Occasionally, there are 2 nearest pressure levels. For example, the standard pressure level is 700 mb; however, there are only 697 mb and 703 mb in the model-produced profile. The distance to 700 mb from 697 mb and 703 mb are the same. In this case, the average of the meteorological variables from the two pressure levels will be used as the variable at the missing standard pressure level. These θ_w and temperature values were further interpolated linearly every 10 minutes to match the radar observation frequency.

2.6 Methodology

Figure 2.3 illustrates the relative position of a small portion of the radar scan relative to the observer at the surface. The polar grid in the figure represents the horizontal positions of 5x5 range bins which are centered over YEG, and over which the radar echoes are averaged and stored in the computer. The grid space in the radar beam is 500 meter. The angle between consecutive radar beams is 0.5° . Each polar grid pixel has a single radar reflectivity value Z . In this study, this area is defined as the sample area of the radar reflectivity factor.

Strictly, to examine the relation between the visibility and reflectivity, the reflectivity factor generated from this area of snow needs to be correlated with the visibility observed in this same snow by an observer at the ground. However, it has been noted that the sample area was at the radar beam height about hundreds of meters above YEG and it might take a few minutes for the snow to reach the ground, depending on the snow size and the beam height. After a few minutes, this sample area might fall to the ground in the same way centered over the observer; or it might drift off away from the observer, depending on the wind condition at the lower level. In addition, it is uncertain when exactly the visibility observation was taken. Regardless, it is chosen to match the radar data with the time stamped on the data time with the visibility at the recorded time in the surface observation (Appendix-B).

It is also noted that there are 25 reflectivity values in the sample area in each observation time. The median value of the reflectivity values in the sample area will be used to correlate with visibility since the median matches the meaning of the “prevailing visibility” from the definition of the visibility.

Positioned in the radar plane, the range from YEG to the radar site is 47.5 km, while the azimuth is 128.2° . So, the length of the arc between 2 rays near YEG is about 0.5 km, and each pixel covers an area of about 0.25 km^2 . The area of the sample area is 2.5 km by 2.5 km, i.e. about 6.25 km^2 .

A major issue when correlating the visibility (recorded every hour) with the 6 hourly accumulated snowfall (recorded every 6 hours) is the difference in sampling time. First, the 6-hourly snowfall is averaged over 6 hours to represent the snowfall rate within the 6 hours because precipitation observations were observed at a 6-hour interval and visibility at hourly intervals. Second, the minimum visibility value in the 6 hours up to and including the time of the precipitation observation is taken and mapped to the snowfall rate. The 6-hourly precipitation amount often contains precipitation of different snow type. To calculate the water equivalent snowfall based on 6-hourly precipitation amount, the following equation is used:

$$S_6 = P \frac{NS}{NP} \quad (18)$$

where S_6 is 6-hourly water equivalent snowfall (mm/6-hours); P is the observed 6-hourly precipitation amount (mm/6-hours); NS is the number of snow reports in 6 hours or reports of snow with any other types of precipitation in 6 hours; NP is the number of hours of reports of all types of precipitation.

To analyze the reduction of visibility caused only by snow, the visibility observations selected to correlate with reflectivity data are those when only snow was reported in the weather group in the hourly observation.

3. Visibility estimations using radar observations

3.1 Visibility – Radar reflectivity scatter plots

In this chapter we explore the relationship between *Vis*-*Z*. Our data set includes all hourly observations of visibility at YEG during the period 31 October 2010 to 30 April which satisfied the following four conditions:

- a) The YEG surface observations were sampled during daylight.
Specifically we have selected only data observed from 1600 to 2300 UTC.
- b) The YEG surface observations indicated the presence of falling snow.
- c) The YEG surface observations indicated an absence of fog or mist
- d) The Carvel radar data had radar reflectivity *Z* observations within 10 minutes of the YEG visibility observations.

With these criteria, there were a total of 1017 (*Z*, *Vis*) acceptable recordings. Figure 3.1 depicts the scatter plot of visibility (*Vis*) versus reflectivity (*Z*). The visibility was measured in units of statute mile (sm) (1 sm = 1.6 km). The *Z* (in units of dBZ) is the median value of reflectivity in the sample area of 5x5 polar grids centered over the Edmonton International Airport (YEG). The scatterplot depicts that there is not a single *Vis*-*Z* curve, but rather a wide scatter. For example, the *Vis* for a given $Z \leq 20$ dBZ had a range from 1 to 15 sm; while the *Vis* for $Z > 20$ dBZ had range from ½ to 8 sm. Alternatively, for a constant *Vis* at 1sm *Z* ranged from 10 dBZ to 35dBZ.

A second indication of the scatter plot is that the degree of scatter in *Vis* (for given *Z*) is smaller with stronger *Z* than it is with weaker *Z*. For example, the *Vis* range is about 14 sm when *Z* value is less than 20 dBZ while *Vis* about 8 sm when *Z* is greater than 20 dBZ. We note that it is not obvious that *Vis* values

decrease with the increase of Z values since some visibility values corresponding to are really high, such as the data points ($Vis \geq 8$ sm, $Z \geq 20$ dBZ).

Table 3.1 list the meteorological observations for the data points that have $Vis \geq 6$ sm despite the fact that there was snowfall ($Z > 20$ dBZ). There were 5 data points occurring on three different days: 4, 7 and 20 January. The soundings indicate that there was no Above Freezing Layer, suggesting that there was no freezing rain at the observation times. The surface temperature values ranged from -1 to -6 °C. The θ_w values at 700mb are about 7-8 °C, suggesting a relatively warm air mass over YEG for January.

What about data points with low Z and low Vis values? Table 3.2 lists meteorological conditions for ($Z < 13$ dBZ, $Vis < 1$ sm) points and ($Z < 10$ dBZ, $Vis < 2$ sm) points. The maximum Z values are listed in the table to see if there were heavy snow spots embedded in the sample area. There are 12 data points select, of which only one data point at 2010:11:17:21:00 is involved with embedded high reflectivity (32.5 dBZ) in the sample area; while the maximum values of other data points are from 12 to 17, very close to 15 dBZ, which suggests very weak snow. Wind speeds are from 3 to 11 kt. The θ_w values at 850mb are about -18°C to -5 °C, indicative of a cold air mass over YEG.

We now examine how the observations recorded at YEG compare to the empirical curves suggested by Rasmussen et al. (1999) and Boudala (2009). Figure 3.2 compares the (Vis , Z) data observed at the YEG with the Rasmussen and Boudala curves. For these curves we have converted the snowfall rates (S) from radar reflectivity (Z) using the empirical Z - S relationship of Sekhon and Srivastava (1970). The Rasmussen and the Boudala curves are broadly consistent with the YEG data in that during snowfall Vis decreases as Z increases. The Rasmussen curve shows a faster reduction in visibility than the Boudala curve.

Comparing the YEG data with these curves suggests that for very weak snowfall (i.e. Z is small) there is a better agreement with the Boudala curve. For example, observation data shows that many Vis values fall within 5 sm when $Z <$

10 dBZ. The *Vis* estimated by the Boudala curve is about 3 - 4 sm, compared to 5 - 8 sm using the Rasmussen curve. For $Z > 20$ dBZ, the *Vis* values estimated by both curves agree well with the YEG observations.

3.2 Probabilistic Visibility estimates based on radar reflectivity

In the introductory chapter (section 1.1) we discussed the need to have probability forecast of weather condition hazardous to aviation. Based on the wide scatter of the (*Vis*, *Z*) data, we attempt to look at the issue as a probability forecasting problem. We intend to use the concept of percentiles to find out the probability of *Vis* with respect to a small range of *Z*. If the 25th percentile is equal to 1 sm for $20 \text{ dBZ} < Z \leq 24 \text{ dBZ}$, it can be interpreted as a 25% probability that the visibility value ≤ 1 sm.

Figure 3.3 is the *box and whisker plot* of *Vis* versus *Z*. The observed *Z* values during snow are divided into bins 4-8, 8-12, 12-16, 16-20, 20-24, 24-28, 28-32, 32-36 dBZ. The center values are 6, 10, 14, 18, 22, 26, 30, and 34, marked on the *Z*-axis. The red horizontal bar denotes the median values. The bottom edge and top edge denote the 25th and 75th percentiles. The interquartile range is the difference between the 75th quartile and the 25th quartile. The length of side edges of the boxes denotes the interquartile ranges (IQRs). The whiskers show the full range of *Vis* values. The horizontal bar at the bottom of the whisker and the horizontal bar at the top of the whisker denote minimum and maximum. The sample sizes of bins (orderly low to high *Z*) are 18, 82, 73, 69, 61, 40, 4, and 3.

Figure 3.3 shows that the median value of *Vis* decreases as *Z* increases. The *Vis* median gradually changes from 3 to $\frac{1}{2}$ sm as the central value of the *Z* bin increases from 6 to 34 dBZ. The *Vis* median values in the boxes quickly decrease as the bin central value changes from 14 to 22 dBZ. The interquartile range (IQR) for $Z < 20$ dBZ ranges from $1\frac{3}{4}$ sm to 3 sm, while the IQR for $Z > 20$ dBZ ranges from $\frac{1}{2}$ sm to $\frac{3}{4}$ sm. The sample sizes for the *Z* bins at 30 and 34 are only 4 and 3 respectively, too small to be included in the discussion. We note that the *Vis* distributions are not the normal distribution since the medians are not at the center

of the boxes. For example, the median is 3 sm at the Z central value equal to 10 dBZ, while the middle value for that box is 3.5 sm. In addition, the long whiskers above the boxes (the upper whiskers) indicate that data are spread mainly for those high visibilities greater than the 75th percentile. Also, the upper whiskers are much longer than the lower whiskers for most box plots. For example, the boxplot at $Z = 10$ dBZ, the upper whisker indicates the visibility range is 10 sm (varying from 5 sm to 15 sm), while the lower whisker the visibility range is about 1½ sm.

Figure 3.4 shows *Box and Whisker plots* of Vis versus Z with the curves marking the 30th, 40th, 50th, and 75th percentiles in black, green, and Magenta respectively. The box-and-whisker's plot is the same as Figure 3.3. The 30th and 40th percentile lines are calculated from the same bin as used in calculating the 25th and 50th and 75th percentiles. The percentile curve is formed by connecting the same p -th percentile (e.g. p equal 25 in the 25th percentile) in each Z bin. The connection between two adjacent points of percentiles can be considered as an interpolation of the percentiles of Vis at Z values between two adjacent center values.

Looking into an individual box-and-whisker's plot (Figure 3.4), e.g., at the center value of $Z = 10$ dBZ, the 30th percentile is 2 sm. The 40th percentile is 2½ sm. The 50th percentile (or the median) is 3 sm. If drawing a line of 1 sm in the figure, this line intercepts the 30th percentile line at Z equal to 18 dBZ, 40th percentile and 50th percentile at Z of 22 dBZ, the 50th percentile at 32 dBZ.

Figure 3.5 compares the relationship of the Vis - Z relationship with the percentile data. For the radar based Vis - S relationship, the equation lines are the same as on Figure 3.2. The red line is the regression equation for Vis - Z relationship based on the observation data used in Figure 3.1. At $Z > 10$, the Vis - Z regression relationship agrees closely with the Boudala curve. For $Z > 12$ dBZ, the visibilities estimated by these two relationships differ by less than ¼ sm. Discrepancy between the Rasmussen curve and the Vis - Z regression equation is more significant. For $Z > 17$ dBZ, the discrepancy is about ½ sm. For $Z \leq 17$ dBZ,

the discrepancy becomes bigger as Z decreases. The biggest difference could be 2.5 sm.

The comparison of the empirical relationships to the percentiles shows that the Vis estimations by empirical relationship are generally above the 50th percentile except for the Rasmussen curve for Z exceeding 23 dBZ.

3.3 Meteorological conditions affecting the Vis - Z relationship

The previous section has shown that a great scatter exist in the relationship between Vis and Z . This section we explore some meteorological factors that could cause this great dispersion.

a) Surface temperature

Figure 3.6 shows the Vis - Z relationship in different surface temperature ranges. Different colors represent different temperature T regimes. In Figure 3.6a, the blue dots represent (Vis, Z) data with $T < -20$ °C; the green squares represent data with $-20^{\circ}\text{C} \leq T < -10$ °C; and the red triangles represent data with $T \geq -10$ °C. The surface temperature data are from hourly surface observation data. Figure 3.6a shows that there is no clustering of (Vis, Z) data according to different temperature groups. Yet, there are some tendencies indicated by the data. Vis values tend to be lower than 6 sm when snow occurred with temperature below -20°C. There are a few exceptions in that some cold regime data had high Vis value for $Z \geq 13$ dBZ. For the intermediate temperature regime (for temperatures between -20°C and -10°C), the Vis values are not very spread and are mainly below 3 sm when Z ranges from 17 to 27 dBZ, and the Vis also tends to be lower than that of the other temperature regimes. For $Z < 17$ dBZ, the Vis values vary from 1sm to 12 sm. For the warm temperature regime (with $T \geq -10^{\circ}\text{C}$), the (Vis, Z) data have a wider spread, when compared to the cold and intermediate temperature regime. For a Z value between 10 and 27 dBZ, the visibilities can range from 1 to 15 sm.

Figure 3.6b shows the results when we use a finer resolution of temperature categories. The results show the same as before. The surface temperature has relatively insignificant effect on the *Vis-Z* relationship.

b) Temperature at 850 mb and 700 mb

Figure 3.7 shows the *Vis-Z* scatterplot for different temperature regimes at 850 mb (a) and at 700 mb (b). Blue dots represent data with $T < -20$ °C; the green squares represent the data with points with -20 °C $\leq T < -10$ °C; the red triangles represent data with $T \geq -10$ °C. The GEMLAM hourly temperature forecast at upper levels at YEG are linearly interpolated into temperatures in a 10 minute interval within one hour. The *Vis-Z* data are the same as in Figure 3.1.

At neither pressure level do the (*Vis*, *Z*) data points cluster according to different temperature ranges. The degrees of scatter in different temperature ranges are different. For cold upper air temperatures, the data points are less scattered. *Vis* values range within 6 sm in the cold temperature regime ($T < -20$ °C) at 850mb, except for a few data points with *Vis* about 6-8 sm as *Z* value is from 14 to 17 dBZ. *Vis* values ≤ 5 sm for $T < -20$ °C at 700mb. The temperature range with most scattering data points at 850mb is the warm regime ($T \geq -10$ °C), while the most spread group at 700 mb is associated with the intermediate temperatures (-20 °C $< T \leq -10$ °C).

c) Web-bulb potential temperature at 850 mb and 700 mb

Figure 3.8 shows the *Vis-Z* relationship for the different θ_w regimes (a) at 850mb (a) and (b) at 700mb. In Figure 3.8a, the blue dots represent data points with $\theta_w < -10$ °C; the green squares represent the data points with -10 °C $\leq \theta_w < 0$ °C; and the red triangles represent the data points with $\theta_w \geq 0$ °C. The observation data are the same as ones used for Figure 3.1. The θ_w values were calculated from hourly forecast temperature, dew point, and pressure at different pressure level from the GEMLAM. Fig 3.8 shows that (*Vis*, *Z*) data points in

different θ_w ranges are overlapped. The θ_w range cannot make the widely spread data points into different clusters.

Fig. 3.8 also shows that the degrees of scatter in different θ_w regimes are different. The data points in the coldest θ_w group are less spread than the data point in the warmer θ_w ranges. At 850mb, most Vis values in the cold θ_w group are mostly below 6 sm. At 700mb, all Vis values from data points in the coldest θ_w regime range are below 6 sm. The Vis values in the intermediate θ_w regime are less scattered than the Vis values in the warmest group. For the intermediate θ_w regime, the Vis values within 5 sm When Z reaches 20 dBZ; however, for the warmest θ_w group, the Vis values range are still 8 sm or greater when Z reaches to about 27 dBZ.

Comparing the data points in the coldest θ_w regime at 850 mb and at 700 mb, it shows some data point with higher visibility values at Z values from 15 to 17 dBZ occur at 850 mb but disappear on 700 mb. That suggests that snow formed in the cold Arctic airmass at 700 mb generally results in low visibility. However, this should be re-examined with more data since the size of the data point in this group is considerably smaller than other groups.

d) Wind

Figure 3.9a shows the (Vis, Z) scatter plot with different wind speed (WS) regimes plotted in different colors. The blue dots represent data with wind speed $WS \leq 5$ kt. The cyan dots represent data with $5 \text{ kt} < WS \leq 10$ kt. The green dots represent data with $10 \text{ kt} < WS \leq 15$ kt. The orange dots represent the data with $WS > 15$ kt. The strongest sustained wind with only snow recorded in the weather group was 22 kt.

The analysis shows that wind speed greater than 15 kt can have significant impact on Vis in snow when Z is greater than about 19 dBZ (Figure 5.9a). When wind speed is weaker than 15 kt, Vis values spread from $\frac{1}{2}$ sm to 15 sm when Z is smaller than 23 dBZ. When wind speed is greater than 15 kt, Vis values still range

from 1 sm to 12 sm. However, when wind speed is greater than 15 kt and Z value is greater than 19 dBZ, most Vis values are within 2 sm.

To examine more closely the relationship between visibility and wind speed, we have re-plotted the data in a scatter diagram of Visibility versus wind speed (Fig 3.9b). Here we plotted visibility versus wind speed at different radar intervals. The blue dots represent (Vis, WS) data for $Z \leq 10$ dBZ. The orange squares represent data for $10 \text{ dBZ} < Z \leq 20$ dBZ. The black triangles represent the data with $Z > 20$ dBZ. Fig. 3.9b shows more clearly the critical wind speed that starts to impact the reduction of visibility by snow. For the reflectivity group of 20 to 30 dBZ, it shows that wind speeds ≥ 12 kt, Vis values are generally below 2.5sm.

3.4 Comparison between day time and night time observations

Figure 3.10 shows the scatter diagram of visibility versus radar reflectivity for Edmonton International Airport (YEG) for the time period 1 October 2010 to 30 April 2011. The data shows both day time and night time observations. As in the previous sections, Z is the median value of reflectivity in a sample area of 5x5 polar grids centered over YEG. The red triangle data are all the (Z, Vis) observed during the day time (specifically from 1600 to 2300 UTC). These data points are the same as those shown in Figure 3.1. The blue dots data show all the observations recorded from 0000 UTC to 1500 UTC. We call this the night time data. The red line ($Vis = 32.5Z^{-1.005}$, $r = -0.46$, $rmse = 3.1$ sm) is the regression equation of relationship between visibility and radar reflectivity using the day time data; the blue line ($Vis = 50.4Z^{-1.02}$, $r = -0.47$, $rmse = 3.9$ sm) denotes the regression equation of relationship between visibility and radar reflectivity using the night time data.

There is a high degree of scatter both during day and night (Figure 3.10). For a given Z value within 22 dBZ, the Vis values from day and night are quite overlapped in the visibility range from 1½ to 15sm. Comparing the two

regression lines, we find that for a given value of radar reflectivity the visibility based on the night time regression curve is higher than the visibility based on the day time regression curve. This suggests that the reduction of visibility due to snow is less apparent during the night time. For $Z < 10$ dBZ, the difference of visibility values estimated by the equation for day and the equation for night is about 2 to 3 sm. For Z from 15 to 20 dBZ, the difference of Vis values estimated by the two equations is about 1 to 2sm. For $Z > 20$ dBZ, the difference between the two equations is about $\frac{1}{2}$ to 1sm.

3.5 Spatial distribution of snow

As discussed in section 2.5, the observations of the reflectivity and visibility were not conducted at the same time and the same location; therefore, we chose the median value from sample grid pixel cells to represent the snow condition to correlate to the surface Vis values. As the median value may not always represent the “best” snow condition at surface where the visibility is recorded at the observation time, some potential bias in the Vis - Z relationship may be involved in our choice of using the median value. In this section, we check how the spacial distribution of snow might impact the scatter of Vis - Z plot.

Table 3.3 lists two examples of the reflectivity values at 5x5 grid pixels centered over YEG at 2100 UTC 27 February 2011 and 2000 UTC 25 October 2010. There is significant variation in radar reflectivity values for the pixels in both cases. For the 27 February case, the radar reflectivity varied from 9.5 dBZ to 39.5 dBZ with a median of 14 dBZ and a standard deviation of 6.7. For The 25 October case, the reflectivity varied from 16.5 dBZ to 22.5 dBZ with a median of 21 dBZ and a standard deviation of 1.5.

Table 3.4 lists the estimated Vis values based on the Z value in each pixel using the day equation for the Vis - Z relationship. The degree of Vis variation over grid pixel cells is dependent on that of Z . For the 27 February case, the visibility values vary from 0.8 to 3.4 sm with a median of 2.5 sm, a standard deviation of 0.6 sm, and the range is 2.6 sm. For the 25 October case, Vis values vary from 1.4

to 1.9sm, with a median of 1.5 sm, a standard deviation of 0.1, and the range is 0.4 sm.

A big range (standard deviation) in radar reflectivity over the grid pixels in the radar sample area results in a big range (standard deviation) of *Vis* values. Comparing the standard deviation of the two cases, we find that standard deviation of *Z* is 6.7 dBZ for 27 February compared to 1.5 dBZ for 25 October. The standard deviations of *Vis* is 0.6 sm for 27 February and 0.1 sm for 25 October.

In Figure 3.11, we further highlight the data points with none of *N* values equal to zero or none of *Z* values equal to -25.5 dBZ in the pixels of the radar sample area. These data points are plotted in red triangles. The blue data points are the whole daytime data (data with one or more *N* values equal to zero or one or more *Z* values equal to -25.5 dBZ plus the data points with none of *N* values equal zero or none of *Z* values equal to -25.5 dBZ in the pixels of the radar sample area in the daytime with only snow recorded in the weather group) in the winter 2010-11. We also plotted the *Vis-Z* regression line to see how well the daytime equation fits to the data points with none of *N* values equal to zero. Figure 3.11 shows that the degree of scatter of data point highlighted in red triangles is much smaller than the one of data with the whole daytime data. For any given *Z* value, the *Vis* range is within 1.5 sm. In addition, the data points are coincidentally very close to the mean line (the *Vis-Z* regression equation line for the daytime data).

3.6 Sensitivity of the *Vis-Z* relationship

We recall that the *Vis-Z* curves used in this section are based on assumptions of a (*Vis-S*) relationship and a (*Z-S*) relationship. Both these choices are empirical relationships and various choices have been suggested by the research literature. In this section we examine the sensitivity of the *Vis-Z* curves based on varying the choices of underlying *Vis-S* and *Z-S* relationships.

Figure 3.12a compares estimated visibility by using different choices for the Vis - S relationship, while keeping the same Z - S relationship. All curves in Figure 3.12a are based on converting radar Z to snowfall S using $Z = 1780S^{2.21}$ suggested by Sekhon et al. (1970). The green curve is computed using $Vis = 0.14S^{-1.55}$ suggested by Richards (1954) for a cold air mass ($\theta_w = 6^\circ\text{C}$). The orange curve is computed using $Vis = 0.43S^{-0.88}$ suggested by Richards (1954) for a warm air mass ($\theta_w = 9^\circ\text{C}$). The blue curve is computed using the Rasmussen et al (1999) relationship for cold air. The black curve is computed using $Vis = 1.3S^{-0.542}$ (Boudala et al, 2008). The blue dots are the (Vis, Z) data observed at YEG, the same as what is shown in Figure 3.1.

Figure 3.12a shows that for a given Z value which will be converted into snowfall rate value using a Z - S relationship, visibilities calculated using different Vis - S relationships are different. For example, when $Z = 10$ dBZ, Vis estimated by Boudala is 3 sm, 3.5 sm by Richards ($\theta_w 9$), 4 sm by Richards ($\theta_w 6$), and 5 sm by Rasmussen. The range among visibilities estimated by different equations decreases as Z value increases until $Z=20$ dBZ. For example, when $Z = 10$ dBZ, the total range among the four estimated visibilities is 2 sm. When $Z = 20$ dBZ, Vis estimated by Richards ($\theta_w 6$) is 1sm, 1.5 sm by Richards ($\theta_w 9$), 2 sm by Rasmussen and Boudala with a range of 1sm among the 4 estimated visibilities. When Z is equal to 30, the range is still close to 1 sm. The difference among rates of Vis diseases with Z is significant within the total Z range from 5 to 35 dBZ. The rate of Vis - S relationships of $\theta_w 6$ is great, so it gives highest visibilities when Z is small and gives the lowest visibilities when Z is bigger. In contrast, the rate of Vis - S relationship by Boudala is small, so it gives lowest visibility with Z is small and highest value when Z is big. Rasmussen gives visibilities higher than ones others give most time while Richards ($\theta_w 6$) gives visibilities lower ones others give most time. In conclusion, for a given Z - S relationship, changing the Vis - S relationship will produce different visibility values. The magnitude of difference in visibility produced by different Vis - S relationship depends on Z when $Z < 20$

dBZ. The magnitude of difference in visibilities produced by different *Vis-S* relationship remains near 1 sm when $Z > 20$ dBZ.

Figure 3.12b compares estimated visibility by using different *Z-S* relationships for dry snow but keeping the same *Vis-S* relationship developed by Rasmussen et al (1999). The green curve is computed using Sekhof et al (1970) *Z-S* relationship. The orange curve is computed using Puhakka's (1975) *Z-S* relationship. The blue curve is computed using Imai's (1960) *Z-S* relationship. The blue dots are the observation data, the same as what is shown in Figure 3.1.

The visibilities calculated using different *Z-S* relationships are different. For a given reflectivity, the visibility based on Imai is lower than one on the Sekhon and Puhakka curves. The difference of visibilities among different *Z-S* relationships is greater when radar reflectivity is weak than the one when reflectivity is strong. For example, the differences are 1.5 sm, 1sm, and $\frac{1}{2}$ sm when Z are 10 dBZ.

In Figure 3.12c, the visibilities corresponding to the black line are calculated using the *Vis-S* relationship suggested by Richards (1954) for a cold air mass ($\theta_w = 6$ °C) and the *Z-S* relationship suggested by Imai (1960) using observed Z . From the discussion above, both equations tend to give visibilities that are lower than ones other equations give. The visibilities denoted by the red line are calculated by the *Vis-S* relationship suggested by Rasmussen et al (1999) and the *Z-S* relationship suggested by Sekhon et al (1970) using observed Z . These two equations tend to give visibilities higher than ones other equations give. By comparing visibilities calculated by these two sets of equations for a given Z , we intend to estimate the max difference of visibilities by choosing different theoretical equations selected in this study. For given Z at 10, 15, 20, 25, 30, 35 dBZ, the visibilities estimated by Richards ($\theta_w,6$)_Imai are 2.5, 1, 0.5, 0.125, near 0 sm; the visibilities calculated by Rasmussen_Sekhon are 5, 3, 1.75, 1, 0.75, within 0.5sm. The differences of visibilities calculated by these two sets of equations are 2.5, 2, 1.25, 0.75, 0.75, and within 0.5 sm. It indicates that the

difference of visibilities calculated by two sets of equations decreases as Z increases.

In conclusion, for a given $Vis-S$ relationship, changing the $Z-S$ relationship yields different visibility estimations. Vice versa, for a given $Z-S$ relationship, changing the $Vis-S$ relationship yields different visibility estimates. The magnitude of difference in visibility estimations depends on Z .

3.7 Summary and discussion

In this section, we have explored the $Vis-Z$ relationship and looked for an approach of forecast probability of visibility. We continue to examine how these estimates are affected by meteorological factors, day-time night time differences, and other factors.

1. The analysis of sensibility of the Vis -Radar-based- S relationship shows that for a given $Z-S$ relationship, changing the $Vis-S$ relationship will produce different visibility estimations. The magnitude of difference in visibilities produced by different $Vis-S$ relationship depends on Z when Z is smaller than 20 dBZ. When Z is greater than 20 dBZ, the magnitude of difference in visibilities produced by different $Vis-S$ relationship remains near 1 sm 20. Furthermore, the magnitude of difference in visibility estimations produced by different $Z-S$ relationships also depends on Z . When Z is greater than 25 dBZ, the magnitude of different is within $\frac{1}{2}$ sm. These results suggest that in estimating snow visibility, the $Vis-S$ relationship and the $Z-S$ relationship are sensitive to each other in estimating snow visibility using radar reflectivity data. The sensibility is higher when Z is smaller and lower when Z is greater.
2. There is a visibility distribution with respect to Z . The analysis of the distribution of visibility with respect to the Z shown in the Box-and-Whisker plots indicates that Median value of Vis decreases as Z

increases. The scatter is largely contributed by the 25 percent points with *Vis* greater than the 75th percentile. The interquartile range with *Z* greater than 20 dBZ is much smaller than the IQR with *Z* value smaller than 20 dBZ.

3. The percentile derived from the *Vis* distribution gives an estimation of the probability of *Vis* which could occur based on a given *Z*. The *Vis* estimation given by the *Vis-Radar-based-snowfall* relationships and the *Vis-Z* regression equation are mostly greater than the 50th percentile.
4. Ranges of surface temperature, the temperatures at 850mb and 700mb, the wet-bulb potential temperatures at 850mb and 700mb cannot separate the wide spread data points into different clusters. This suggest that surface temperature, the temperature at 850 mb and 700 mb, and the wet-bulb temperature at 850 mb and 700 mb are not the determine factors to impact the wide spread in the *Vis-Z* relationship in this data set.
5. Data points are generally less spread with colder temperature or θ_w , more spread with warmer temperature or θ_w except for temperatures at 700 mb. At 700 mb, the most spread data group is associated with the middle temperature ranges from -20 to -10 °C. The data is least spread when the surface temperature or the temperature at 850mb, or the temperature at 700 mb is below -20°C, or the potential wet bulb temperature at 850 mb below -10°C, or the θ_w at 700mb below 0°C. The temperature at 700mb is below -20°C, or web-bulb potential temperature at 700 mb below 0 °C, the *Vis* values in falling snow with detectable reflectivity are mostly near to below 3 sm except for *Z* values smaller than 10 dBZ.
6. The impact of strong winds on visibility is evident only when wind speed > 15 kt and reflectivity > 19 dBZ.

7. On average, the *Vis* value with the day observation time for a given *Z* value is lower than the *Vis* value from the night observation time for the same *Z* value.
8. There is a great variation of equivalent reflectivity factor over the radar sample area. This variation results in the variation of calculated visibilities for the pixels over the sample area. If instead of the median value, the other value in the sample area could be better to represent the true snow condition where and when the observation of *Vis* is taken, the visibility observation value would not be close to the median value of the calculated *Vis* values. In this sense, the median reflectivity over the sample area would not be a best value to represent the snow when the visibility value observed at the time and errors would be introduced into the *Vis*-*Z* relationship. The bigger the variation of equivalent reflectivity factor, the bigger the error could be. Assuming that the distribution of *Z* values in the grid pixels over the sample area represent the distribution of snow, this result suggests that a part of contribution of scatter come from the snow distribution itself and the nature of correlating of two sets of data measured not simultaneously at different places.

4. Visibility and snowfall

4.1 Snow conditions from 1 October 2006 to April 30 2011

In the previous chapter we have analyzed the relationship between visibility and radar reflectivity at Edmonton International Airport. Our entire analysis was based on the data observed within the period 1 October 2010 to 31 April 2011. It is a fair question whether the results from this one winter season are representative also for other years, or whether the selected period is special. It would be best to repeat the Visibility-radar reflectivity analysis for other winter seasons as well. However, the radar archive system for radar measurements cannot easily be used to download the digital data as an outside user. It has to be done by a person requiring many hours. As we did not have the resources for doing this, we had to rely on a single season of digital radar data. However, 6-hourly snowfall estimates are readily available for recent years and can be quickly taken from the Environment Canada climate archive. Based on the availability of 6 hourly snowfall accumulation data at YEG, a visibility-snowfall analysis is made for four winter seasons. The underlying rationale is that if the *Vis-S* relationship for the 2010 /2011 winter turns out to be similar to the other three winters, then it is likely that *Vis-Z* relationship based on the 2010/ 2011 winter observations should also hold for other years.

Table 4.1 lists the amount of snowfall, the number of snow days, the number of snow hours, and the number hours with visibility observation value ≤ 5 sm, 3 sm, 2 sm, and 1 sm, respectively. The snowfall is given in *Water Equivalent Snowfall* (WES: snowfall melted into water and measured in mm). The amount of WES is calculated using 6-hour precipitation amount. If multiple types of precipitation exist within the 6 hours, the WES is determined using the 6-hour precipitation amount multiplied by the ratio of number of snow reported to the total number of precipitation reported, as described in the section of 2.5 (c). The number of snow days was computed data with snow (also including snow mixed with other types of precipitation) recorded in the weather group at any time during

the day. The number of snow hours was computed using data with snow including snow mixed with other types of precipitation recorded in the weather group in the observation hours. Because this study will deal with the reduction of visibility by snow, the number of hours of visibility less than or equal to 5 sm, 3 sm, 2 sm, and 1 sm were calculated using data with only snow recorded in the weather group in the hourly observation data in the winters from year 2006-07 to 2010-11..

This table shows that the winter of 2010-11 had highest snowfall, most snow days, snow hours, and most hours of $Vis \leq 5$ sm, 3 sm, 2 sm, and 1sm compared to the other years. From October 2010 to April 2011, the total WES amount was 124 mm, the greatest snow amount in the 5 winters. This is 30 mm greater than 92 mm (the average of the snow amount of 5 winters), about 20 mm more than the second most (102 mm); and about 45 mm greater than 78 mm (the least amount of WES in the winter of 2007-08). The number of snow days in the winter 2010-11 is 97, 7 days more than the average of snow days of the 5 winters, one day shorter than 97 days (the most snow days in the winter 2006-07), and 15 days more than 82 days (the fewest days in the winter 2009-10). The number of hours of snow reported during the winter of year 2010-11 is about 1090, the highest among the 5 winters. It is about 230 hours higher than 860, the average over the 5 winter and about 285 hours more than 705 hours, the lowest number in the 5 winters.

The number of hours with Vis smaller than or equal to 5 sm in the winter 2010-11 is about 320 hours, about 90 hours more than 230 hours (the average over the 5 winters); about 65 hours more than the second most. It is about 180 hours more than 139, the lowest number among the 5 winters. The number of hours with Vis smaller than or equal to 3 sm in the winter 2010-11 is about 132 hours, the highest number among the 5 winter. It is about 30 hours more than the average over the 5 winters (91 hours); about 30 hour more than the second most (94 hours). It is about 75 hours more than 55, the lowest number among the 5 winters. The number of hours with Vis equal or small that 2 sm in the winter 2010-11 is about 67 hours, the highest number among the 5 winter. It is about 20

hours more than 45 hours, the average number over the 5 winters. It is also about 20 hours more than the second most, which is also 45 hours. It is 35 hours more than 32, the lowest number among the 5 winters. The number of hours with *Vis* smaller than or equal to 1 sm in the winter 2010-11 is about 14 hours, the highest number among the 5 winters. It is 6 hours more than 8 hours, the average number over the 5 winters, only one hour more than the second most. It is 11 hours more than 3, the lowest number among the 5 winters.

Table 4.2 shows that within the winter 2010-2011, the WES, the number of snow hours, and the numbers of hours of *Vis* smaller than or equal to 5 sm, 3 sm, 2 sm in Jan. 2010 were much greater than those in other winter months. Within the winter 2010-11, the higher WES occurred from December 2010 to March 2011, and these values are 19 mm, 47 mm, 15 mm, and 16 mm respectively. The highest value of WES is 47 mm, occurring in January 2011, more than twice the amount of the WES values in the other months. The higher numbers of snow days range from 20, 23, 15, and 20, occurring from December 2010 to March 2011. The higher numbers of snow hours are 124, 210, 300, 137, 241 hours from November 2010 to Mar. 2011. The highest number is 300 hours in January 2011, about 60 hours higher than the second highest number. The higher numbers of hours $Vis \leq 5$ sm are 30, 36, 133, 56, 44 hours from November 2010 to March 2011. The higher numbers of hours $Vis \leq 3$ sm are 10, 18, 61, 21, 9, 12 hours from November 2010 to April 2011.

Comparing the WES in the winter 2010-11 with the monthly average over 5 winter years, the WES (Table 3.3), it shows that the number of snow hours, the numbers of hours of *Vis* smaller than or equal to 5 sm, 3 sm, 2 sm in January in the winter 2010-11 are greater than the monthly averages of those values.

Comparing the WES in the winter 2010-2011 with the average over the 5 winters, the WES in January in the winter 2010-11 is about 30 mm greater than 18.2, the average value. The 30 mm is also the amount WES of the winter 2010-2011 excess the average yearly WES over five winters. The number of snow days in January in the winter 2010-11 is 23 days, 6 days more than the average value. The

number of snow hours in January in the winter 2010-11 is 300 hours, about 125 hours more than the average value. The number of snow hours of Vis smaller than or equal to 5 sm in January in the winter 2010-11 is 133 hours, about 85 hours more than the average value which 46 hours. The number of snow hours of Vis smaller than or equal to 3 sm in January in the winter 2010-11 is 133 hours, about 87 hours more than the average value. The number of snow hours $Vis \leq 2$ sm in January in the winter 2010-11 is 28 hours, about 20 hours more than the average value.

In summary, the snowfall in the winter 2010-11 is about 30 mm more than the 5-years' average of about 90 mm. The excessive snowfall was mainly contributed from the snowfall in January 2011. More snowfall in 2010-11 generated more numbers of snow hours, and hours with low visibilities.

4.2 Vis - S relationship for the winters 2006 to 2011

We have only one year of radar data, but 5 years of 6 hourly precipitation data and 6 years of hourly observation data. We want to see if the snow in the winter of 2010-11 is similar to the snow in the other 4 years so that the result of Vis - Z analysis in the one winter may be representative to the other years.

Figure 4.1 shows the comparison of the empirical Vis - S relationships to the observed Vis - S data for the five winter seasons from 2006-07 to 2010-11. The precipitation rate (mm/hr) is the averaged 6-hourly precipitation. The visibility (sm) is the minimum visibility value of the 6 visibilities observed 6 hours before the observation times for precipitation (00, 06, 12, 18 UTC). The blue dots denote the Vis - S relationship using data observed at 0600 UTC and 1200 UTC (i.e. night-time observations), and the red triangles denote the Vis - S relationship using data observed at 1800 UTC and 0000 UTC (i.e. day-time observations). The solid curves in green, cyan, and red denote the Vis - S equations of Richards (green), Rasmussen (cyan), and Boudala (red). The data sizes are 32, 24, 25, 21, and 46 for the winter of 2006-07, 2007-08, 2008-09, 2009-10, and 2010-11, respectively.

Figure 4.1 shows that more night data points occur at the top of each figure and more daytime day data occur at the bottom of each scatter diagram. This suggests that the *Vis* observed during day tends to be lower than the values observed at night for the same snowfall rate. This trend is apparent in all 5 years. The scatter on all diagrams is significant, particularly for the night-time data. There are more data points in the winter of 2010-11 than other winter seasons. The number of events with the precipitation rate greater than 0.5 mm/h for 2010-11, is 4 more compared to the other years. In summary, snow in the winter of 2010-11 was similar with the other years except that there were more snow events and slightly more heavy snow events.

4.3 Airmass analysis

It was identified that the period 1 October 2010 to 31 April 2012 had more snow compared to the previous four winter seasons. It is thus interesting to identify the type of air mass that was generating the heavy snowfall. Figure 4.2 shows the time series of wet bulb potential temperature (θ_w) at 925 mb (blue), 850 mb (cyan), 700 mb (magenta), and 500 mb (red) from 1 October 2010 to 30 April 2012. The θ_w values were computed from the Stony Plain sounding data observed at 0000 UTC and 1200 UTC. The green dots in the figure show the YEG hourly visibility observations (with only snow in the weather group) .

The θ_w values at the higher altitudes are greater than θ_w values from lower altitudes, indicating that the atmosphere was stable for moist convection. θ_w values at lower levels (925mb and 850mb) fluctuate greatly and the magnitude of the fluctuation is about 30 °C from -20 to 10°C. However, the θ_w values at 500mb fluctuate less over the season (from about 0°C to 15 °C). During most snow events, θ_w values at 700 mb are near or below 7 degree Celsius, mostly ranging from -5°C to 5°C, at 500 mb from 10°C to 0°C.

Figure 4.3 plots the time series of temperature at 925 mb (blue), 850 mb (cyan), 700 mb (magenta), and 500 mb (red) plotted with visibility data (with only snow in the weather group) from Stony Plain soundings observed at 0000 UTC

and 1200 UTC. The green dots show the YEG hourly visibilities observations (when only snow is recorded in the weather group). It is desirable to identify melting band conditions as wet snow can contaminate the radar observations. The observations show that usually the temperatures from 925 to 500mb stayed below 0°C. There were few exceptions, with above freezing temperatures at 850 mb: 18-23 January 2011, and 12-17 February 2011. During these two periods, the 925mb temperature was about 0° C, and the 850 mb temperature about 3°C. There was no precipitation during these warm spells.

4.4 Summary

In summary, although the total WES in the winter 2010-11 is more than other years in the five winters from 2006-07 to 2010-11, scatter born in the *Vis-S* relationship are consistent in the five years. The excessive snowfall in 2010-11 was mainly contributed by the snowfall in Jan. 2011. Much snowfall in 2010-11 generated more numbers of snow hours, and hours with low visibilities, which increased the size of radar dataset.

5. Conclusions and recommendations

5.1 Summary and conclusions

Snow is an important weather phenomenon that impacts visibility. Visibility is a crucial element for aviation operations. Forecasting visibility reduced by snow is challenging to weather forecasters. In this thesis, we have explored the possibility approach to estimate visibility (Vis) at the Edmonton International Airport in an operational setting by using the observed radar reflectivity factor (Z) at Carvel and the hourly surface observation visibility measurements from 1 October 2010 to 30 April 2011. We used percentiles derived from the visibility distribution to estimate the probability based on a given reflectivity bin. The 30%, 40%, 50%, and 75% distributions were examined. The 50% distribution (i.e. the median value) decreases as Z increases. The best fit to the (Vis , Z) observation data was found to be:

$$Vis = 32.46Z^{-1}, \quad (19)$$

with the correlation coefficient $r^2 = 0.45$.

We have also investigated the impacts of weather conditions on the Vis - Z relationship. We have found that the (Vis , Z) relationship is not dependent on the profile of temperature and wet-bulb potential temperature. However, strong winds greater than 15 knots significantly affect visibility when reflectivity greater than 19 dBZ.

The accuracies of empirical relationships between *visibility* and *snowfall-rate* (S) based Carvel radar observations were also tested. We have found that the Boudala's method using the Sekhon's Z - S (snowfall rate) relationship for the radar based snowfall rate agreed closely with the best-fit to the observation. However, visibility estimates made by both Boudata's method and Rasmussen's method were mostly greater than the 50th percentile.

As a forecaster myself, I perceive that some of these findings can be used in nowcasting visibility during snow by using the radar reflectivity factors observed in the upstream area of weather. The probability distribution of visibility for radar reflectivity bins can assist in making visibility estimates. If I see the median of the reflectivity values greater than 20 dBZ, I would be more confident about the estimates of the probability of visibility and give a forecast with a small range of visibility because the interquartile ranges are smaller when Z is greater than 20 dBZ. In addition, I will zoom into the upstream area on the radar image and look into the variation of the reflectivity factors. If all pixels in the area are filled with radar echoes from the precipitation, then, the visibility should be very close to the estimates by the $Vis - Z$ regression equation.

We conclude that the Carvel radar provides useful information about visibility at YEG during snowfall, but it is *not* a substitute for a human observer.

5.2 Limitations and recommendations for further studies

The analysis in this thesis is based on one winter of observations for a single location. This is a relatively small data set for such an investigation, particularly for heavy snowfall occurrences. To expand the data set to have more samples would be useful. We recommend that similar research should be carried out using a multiple year data set. Furthermore, it would be interesting to widen the study to other airport locations.

In this study we only had 6-hourly snowfall measurements at YEG. It would be valuable if we would have snowfall measurements taken every 10 minutes or so, to be consistent with the time resolution of the radar data. We recommend to utilize a snow measurements using the latest LIDAR technology or otherwise to obtain suitable snowfall rate measurement for Canadian airports.

In this study, we assume that snow represented by the radar sample area centered over YEG at the radar scanning level would be the snow observed at YEG by the observer. This may not always be the best assumption, because

strong winds could transport the snowflakes off the YEG observation site. It would be interesting to explore whether there could be suitable adjustment made to allow for lateral movement of snow.

The findings of this thesis are based entirely on data analysis of observations. To determine a suitable *Vis* - *Z* relationship it would be interesting to conduct a modelling study in which we model the extinction properties of falling model ice crystals. A combined observation-modelling approach may offer the best tool to derive a useful *Vis* – *Z* relationship to be used for aviation meteorology.

Tables

Table 1.1: Some of the Vis - S (*snowfall*) relationships in the literature (Rasmussen, 1999; Boudala, 2010; Richards, 1954, (see Appendix A)) to be tested.

| Author | Vis | Unit |
|------------------|--|---------------------------------------|
| Rasmussen (1999) | $Vis = 2.21 * S^{-1} \quad (T \leq 0)$ | Vis : cm; S : cms^{-1} |
| Boudala (2010) | $\log(\sigma) = 0.837 + 0.542 \log(S)$; $Vis = 3 / \sigma$ | Vis : km; S : mm hr^{-1} |
| Richards (1954) | $Vis = 0.14S^{-1.55} \quad (\theta_w = 6 \text{ } ^\circ\text{C})$ | Vis : sm; S : mm hr^{-1} |
| Richards (1954) | $Vis = 0.43S^{-0.88} \quad (\theta_w = 9 \text{ } ^\circ\text{C})$ | Vis : sm; S : mm hr^{-1} |

Table 1.2: Z - S relationships from the literature (cited by Rasmussen, 2003). Z is the reflectivity factor in dBZ; S is snowfall rate in mm hr^{-1} .

| Author | $Z =$ |
|------------------------------|---|
| Imai (1960) | $540S^2 \quad (\bar{T}^* < 0 \text{ } ^\circ\text{C})$ |
| Puhakka (1975) | $1050S^2 \quad (\bar{T}^* < 0 \text{ } ^\circ\text{C})$ |
| Sekhon and Srivastava (1970) | $1780S^{2.21}$ |

\bar{T}^* = mean air temperature

Table 2.1: Data sets used in this study. YEG: Edmonton International Airport; WSE: Stony Plain Upper Air Station; T : Temperature; θ_w : wet-bulb potential temperature.

| Datasets | Variables | Time Resolution |
|--------------------------|--------------------|-----------------|
| YEG surface observation | visibility | 1 hour |
| | temperature | |
| | wind | |
| | wind direction | |
| | Weather types | |
| YEG precipitation amount | snow fall amount | 6 hours |
| Carvel radar data | radar reflectivity | 10 minutes |
| WSE soundings | T , θ_w | 12 hours |
| YEG model sounding | θ_w | 1 hour |

Table 2.2: A small portion of Hourly meteorological observations recorded at the YEG airport from 3 Feb. 2011 to 5 Feb. 2011. The table lists Ceiling (height from the surface to the base of a layer of clouds aloft in 30's meter), *Vis* (prevailing visibility in km), wind direction (degree), wind speed (km hr⁻¹), gust speed (km hr⁻¹), dry bulb (dry-bulb temperature or temperature in °C), wet bulb (wet bulb temperature in °C), dew point (°C), RH (relative humidity in percentage), MSL press (mean sea level pressure in kPa), station pressure (station pressure in kPa), cloud opacity (tenth), and cloud amount (tenth). The last column lists the weather types (RW-, light rain shower; S-, light snow; single -, no weather reported).

| YYYY-MM-DD-HH:MM LST | Ceiling | | Wind | Wind | Gust | Dry | Wet | Dew | RH | MSL | Station | Cloud | Cloud | Weather |
|----------------------|---------|------|-----------|-------|-------|-------|-------|-------|-----|-------|---------|---------|--------|---------|
| | 30's m | km | Direction | Speed | Speed | Bulb | Bulb | Point | % | Press | Press | Opacity | Amount | |
| | | | 10's deg | km/hr | km/hr | deg C | deg C | deg C | | kPa | kPa | tenths | tenths | |
| 2011/02/03/ 22:00 | 57 | 24.1 | 26 | 9 | | 2.4 | 1.9 | 1.3 | 92 | 101.4 | 92.72 | 9 | 10 | - |
| 2011/02/03/ 23:00 | 60 | 24.1 | 22 | 17 | | 2.7 | 2.0 | 1.2 | 90 | 101.4 | 92.73 | 10 | 10 | - |
| 2011/02/03/ 23:18S | 42 | 24.1 | 23 | 15 | | 2.4 | | | | | | | | RW- |
| 2011/02/04/ 00:00 | 29 | 24.1 | 24 | 15 | | 3.3 | 2.6 | 1.7 | 89 | 101.4 | 92.76 | 10 | 10 | RW- |
| 2011/02/04/ 01:00 | 50 | 19.3 | 25 | 9 | | 1.9 | 1.8 | 1.6 | 98 | 101.4 | 92.76 | 10 | 10 | RW- |
| 2011/02/04/ 02:00 | 42 | 24.1 | 21 | 6 | | 1.6 | 1.6 | 1.6 | 100 | 101.3 | 92.69 | 10 | 10 | RW- |
| 2011/02/04/ 02:13S | 75 | 24.1 | 17 | 9 | | 1.8 | | | | | | | | - |
| 2011/02/04/ 03:00 | 86 | 24.1 | 19 | 11 | | 1.5 | 1.5 | 1.5 | 100 | 101.2 | 92.60 | 8 | 8 | - |
| 2011/02/04/ 04:00 | 150 | 24.1 | 19 | 13 | | 1.8 | 1.7 | 1.5 | 98 | 101.1 | 92.48 | 9 | 9 | - |
| 2011/02/04/ 05:00 | 160 | 24.1 | 19 | 15 | | 2.0 | 1.5 | 0.9 | 92 | 101.0 | 92.42 | 10 | 10 | - |
| 2011/02/04/ 06:00 | 180 | 24.1 | 18 | 11 | | 1.4 | 0.9 | 0.1 | 91 | 100.9 | 92.31 | 10 | 10 | - |
| 2011/02/05/ 16:00 | 28 | 19.3 | 35 | 33 | 46 | -5.0 | -5.2 | -6.2 | 91 | 102.7 | 93.89 | 9 | 10 | S- |
| 2011/02/05/ 16:27S | 13 | 3.6 | 35 | 28 | | -5.0 | | | | | | | | S- |
| 2011/02/05/ 16:49S | 20 | 4.8 | 35 | 37 | | -6.0 | | | | | | | | S- |
| 2011/02/05/ 17:00 | 19 | 4.8 | 35 | 35 | 44 | -6.2 | -6.5 | -7.8 | 88 | 102.9 | 94.03 | 10 | 10 | S- |
| 2011/02/05/ 17:33S | UNL | 24.1 | 34 | 39 | 48 | -7.6 | | | | | | | | - |
| 2011/02/05/ 17:53S | 43 | 19.3 | 34 | 28 | 39 | -7.8 | | | | | | | | S- |

Table 3.1: Summary of reflectivity parameters (Z : the median value in the radar sample area; Min: the minimum) and some meteorological parameters (Vis : visibility; WS : wind speed; T_{sfc} : surface temperature; θ_w 850: θ_w at 850mb, θ_w 700: θ_w at 700mb; T_{850} : temperature at 850mb; T_{700} : temperature at 700mb) selected from the data used in Figure 3.1 with selection criteria: $Z \geq 20$ dBZ, and visibility > 6 sm).

| Observation time (year:mm:d:h:mi) in UTC | Z | Min (dBZ) | Vis (sm) | WS (kt) | T_{sfc} ($^{\circ}C$) | θ_w 850 ($^{\circ}C$) | θ_w 700 ($^{\circ}C$) | T_{850} ($^{\circ}C$) | T_{700} ($^{\circ}C$) |
|--|------|--------------|---------------|--------------|------------------------------|-----------------------------------|-----------------------------------|------------------------------|------------------------------|
| 2011:01:04:19:00 | 28 | -25.5 | 15 | 14 | -1.2 | 4.0 | 7.0 | -3.1 | - |
| 2011:01:07:18:50 | 20.5 | -25.5 | 15 | 11 | -4.7 | 2.3 | 7.7 | -4.2 | -9.6 |
| 2011:01:07:19:00 | 22 | -25.5 | 10 | 11 | -4.7 | 2.3 | 7.8 | -4.1 | -9.5 |
| 2011:01:20:18:00 | 24.5 | -25.5 | 8 | 11 | -8.3 | 4.4 | 7.1 | -2.0 | - |
| 2011:01:20:19:00 | 27.5 | -25.5 | 8 | 6 | -6.4 | 5.1 | 7.1 | -2.3 | - |

Table 3.2: Summary of reflectivity factor parameters (Z : the median value in the radar sample area; Max: the maximum) and some meteorological parameters (ceiling: height from the surface to the base of a layer of clouds; Vis : visibility; WS: wind speed; T_{sfc} : surface temperature; θ_w 850: θ_w at 850mb, θ_w 700: θ_w at 700mb; T850: temperature at 850mb; T700: temperature at 700mb) selected from the data used in Figure 3.1 with the selection criteria: $Z < 13$ dBZ and $Vis < 1$ sm or $Z < 10$ dBZ and $Vis < 2$ sm.

| Observation time (Year:mm:d:h:mi) in UTC | Z | Max (dBZ) | Ceiling (ft) | Vis (sm) | WS (kt) | T_{sfc} (°C) | θ_w 850 (°C) | θ_w 700 (°C) | T850 (°C) | T700 (°C) |
|--|------|--------------|-----------------|---------------|------------|-------------------|------------------------|------------------------|--------------|--------------|
| 2010:11:17:21:00 | 10.5 | 32.5 | 2434 | 1.0 | 10 | -11.0 | -8.3 | 2.3 | -18.1 | -18.2 |
| 2011:01:09:23:50 | 6.5 | 16.5 | 1927 | 2.0 | 10 | -16.0 | -10.5 | 0.5 | -20.0 | -19.8 |
| 2011:01:12:18:30 | 8.5 | 12 | 2535 | 2.0 | 3 | -25.1 | -6.7 | 2.0 | -16.4 | -18.7 |
| 2011:01:12:23:20 | 8.5 | 14.5 | 4259 | 1.5 | 6 | -23.7 | -9.5 | 3.0 | -19.6 | -16.3 |
| 2011:01:14:21:30 | 9 | 14 | 2535 | 1.5 | 7 | -25.1 | -17.8 | 2.4 | -27.6 | -17.4 |
| 2011:01:16:18:00 | 10.5 | 15.5 | 710 | 0.7 | 7 | -20.8 | -12.2 | 8.8 | -21.8 | -8.6 |
| 2011:01:19:20:40 | 6.5 | 18 | 6490 | 2.0 | 6 | -10.1 | -5.7 | -0.5 | -13.9 | -22.0 |
| 2011:02:27:21:40 | 7 | 12 | 1622 | 1.5 | 14 | -14.6 | -9.1 | 0.5 | -19.1 | -19.1 |
| 2011:02:28:19:30 | 10.5 | 15 | 710 | 0.6 | 11 | -24.1 | -18.3 | -5.2 | -28.1 | -25.8 |
| 2011:02:28:20:20 | 10.5 | 17.5 | 913 | 0.7 | 10 | -24.1 | -18.4 | -5.9 | -28.1 | -26.5 |
| 2011:02:28:21:50 | 9.5 | 14.5 | 1521 | 1.0 | 11 | -24.2 | -18.1 | -6.2 | -28.4 | -26.6 |
| 2011:02:28:22:40 | 8 | 14 | 2028 | 1.2 | 8 | -23.8 | -18.2 | -6.5 | -28.9 | -26.9 |

Table 3.3: The reflectivity factor (dBZ) value at each grid pixel in the 5x5 grid sample area centered over YEG at 2011:02:27:21:00 UTC and 2010:10:25:20:00 UTC. The median value and standard deviation of the sample at 2011:02:27:21:00 UTC are 14 dBZ, and 6.7 respectively. The median value and standard deviation at 2010:10:25:20:00 UTC are 21 dBZ, and 1.5 respectively.

| Reflectivity (dBZ) in each grid cell at 2011:02:27:21:00 UTC | | | | | Reflectivity (dBZ) in each grid cell at 2010:10:25:20:00 UTC | | | | |
|--|------|------|------|------|--|------|------|------|------|
| 23.5 | 13.0 | 11.0 | 11.5 | 9.5 | 19.5 | 22.5 | 16.5 | 21.5 | 21.5 |
| 39.5 | 16.5 | 16.0 | 11.5 | 13.5 | 21.5 | 21.0 | 22.5 | 21.5 | 21.5 |
| 18.5 | 14.0 | 16.5 | 13.5 | 15.5 | 20.5 | 22.5 | 18.5 | 18.5 | 19.5 |
| 16.0 | 14.0 | 14.0 | 15.0 | 12.5 | 21.0 | 22.5 | 21.5 | 21.5 | 19.5 |
| 31.5 | 10.0 | 14.5 | 13.0 | 11.0 | 19.0 | 21.5 | 18.5 | 20.5 | 20.5 |

Table 3.4: Estimated *Vis* (unit: sm) value at each grid pixel (unit: dBZ) in a 5x5 grid sample area centered over YEG at 2011:02:27:21:00 UTC and 2010:10:25:20:00 UTC. The *Vis*-*Z* equation for the *Vis* estimation: $Vis=32.5*Z^{1.0}$, $r=-0.46$, $rmse=3.1sm$. The *Z* values are from Table 3.3. The median value and standard deviation of *Vis* of the sample at 2011:02:27:21:00 UTC are 2.9sm, and 0.6 respectively. The median value and standard deviation of *Vis* of the sample at 2010:10:25:20:00 UTC are 1.5, and 0.1 respectively.

| Calculated <i>Vis</i> (sm) value in each grid cell at 2011:02:27:21:00 UTC | | | | | Calculated <i>Vis</i> (sm) value in each grid cell at 2010:10:25:20:00 UTC | | | | |
|--|-----|-----|-----|-----|--|-----|-----|-----|-----|
| 1.4 | 2.5 | 2.9 | 2.8 | 3.4 | 1.6 | 1.4 | 1.9 | 1.5 | 1.5 |
| 0.8 | 1.9 | 2.0 | 2.8 | 2.4 | 1.5 | 1.5 | 1.4 | 1.5 | 1.5 |
| 1.7 | 2.3 | 1.9 | 2.4 | 2.1 | 1.6 | 1.4 | 1.7 | 1.7 | 1.6 |
| 2.0 | 2.3 | 2.3 | 2.1 | 2.6 | 1.5 | 1.4 | 1.5 | 1.5 | 1.6 |
| 1.0 | 3.2 | 2.2 | 2.5 | 2.9 | 1.7 | 1.5 | 1.7 | 1.6 | 1.6 |

Table 4.1: The amount of water equivalent snowfall (WES), the number of days, the number of hours with snow recorded in the weather group, the number of hours with *Vis* reported ≤ 5 sm, 3 sm, 2 sm, and 1 sm and with only snow recorded in the weather group in the winters from 2006-07 to 2010-11 at YEG.

| Parameters | yr06-07 | yr07-08 | yr08-09 | yr09-10 | yr10-11 | Average |
|------------------------------|---------|---------|---------|---------|---------|---------|
| WES (mm) | 102.1 | 77.9 | 78.6 | 78.4 | 123.6 | 92.1 |
| Snow Days | 98 | 88 | 85 | 82 | 97 | 90 |
| Snow Hours | 899 | 705 | 728 | 875 | 1091 | 860 |
| Hours <i>Vis</i> ≤ 5 sm | 257 | 226 | 204 | 139 | 321 | 230 |
| Hours <i>Vis</i> ≤ 3 sm | 94 | 94 | 80 | 55 | 132 | 91 |
| Hours <i>Vis</i> ≤ 2 sm | 45 | 43 | 37 | 32 | 67 | 45 |
| Hours <i>Vis</i> ≤ 1 sm | 3 | 3 | 4 | 13 | 14 | 8 |

Table 4.2: The amount of water equivalent snowfall (WES), the number of days with snow recorded in the weather group, the number hours with snow recorded in the weather group, the number of hours with *Vis* reported ≤ 5 sm, 3 sm, 2 sm, and 1sm and with only snow recorded in the weather group in the winter months of 2010-11 at YEG.

| Parameters | Oct 2010 | Nov 2010 | Dec 2010 | Jan 2011 | Feb 2011 | Mar 2011 | Apr 2011 | May 2011 | Total |
|------------------------------|----------|----------|----------|----------|----------|----------|----------|----------|-------|
| WES (mm) | 3.9 | 13.0 | 19.3 | 47.3 | 15.3 | 16.0 | 8.8 | 0.0 | 123.6 |
| Snow Days | 5 | 10 | 20 | 23 | 15 | 20 | 4 | 0 | 97 |
| Snow Hours | 38 | 124 | 219 | 300 | 137 | 241 | 32 | 0 | 1091 |
| Hours <i>Vis</i> ≤ 5 sm | 7 | 30 | 36 | 133 | 56 | 44 | 15 | 0 | 321 |
| Hours <i>Vis</i> ≤ 3 sm | 1 | 10 | 18 | 61 | 21 | 9 | 12 | 0 | 132 |
| Hours <i>Vis</i> ≤ 2 sm | 0 | 2 | 12 | 28 | 11 | 4 | 10 | 0 | 67 |
| Hours <i>Vis</i> ≤ 1 sm | 0 | 0 | 5 | 3 | 3 | 1 | 2 | 0 | 14 |

Table A-1: Precipitation rate values (S) and visibility values (Vis) read from the equations lines plotted on Figure 1.2.

| $\theta_w,06$ | | $\theta_w,09$ | | $\theta_w,12$ | | $\theta_w,15$ | |
|---------------|------------|---------------|------------|---------------|------------|---------------|------------|
| S (mm/hr) | Vis (sm) |
| 0.1 | 2 | 0.1 | 3.5 | 0.25 | 2.375 | 0.5 | 2.05 |
| 0.25 | 1.05 | 0.105 | 3 | 0.5 | 1.72 | 0.75 | 1.75 |
| 0.5 | 0.75 | 0.11 | 2.5 | 0.75 | 1.425 | 1 | 1.5 |
| 0.75 | 0.5 | 0.12 | 2 | 1 | 1.175 | 1.25 | 1.3 |
| 1 | 0.33 | 0.125 | 1.875 | 1.25 | 0.972 | 1.5 | 1.125 |
| 1.25 | 0.125 | 0.25 | 1.58 | 1.5 | 0.8 | 1.75 | 1.02 |
| 1.5 | 0.01 | 0.5 | 1.23 | 1.75 | 0.625 | 2 | 0.875 |
| | | 0.75 | 1 | 2 | 0.48 | 2.25 | 0.75 |
| | | 1 | 0.75 | 2.25 | 0.375 | 2.5 | 0.625 |
| | | 1.25 | 0.54 | 2.5 | 0.27 | 2.75 | 0.52 |
| | | 1.5 | 0.4 | 2.75 | 0.175 | 3 | 0.3965 |
| | | 1.75 | 0.275 | 3 | 0.075 | 3.25 | 0.3125 |
| | | 2 | 0.156 | 3.25 | 0.05 | 3.5 | 0.175 |
| | | 2.25 | 0.125 | | | 3.75 | 0.125 |
| | | 2.45 | 0.1 | | | 4 | 0.0625 |
| | | | | | | 4.25 | 0.09 |

Table A-2: Correlation coefficients and coefficients of the best-fitting based on the data listed in Table A-1. r is correlation coefficient; a and m are referred to coefficients in the equation A-1.

| | r | m | a |
|---------------|----------|----------|----------|
| $\theta_w,06$ | -0.80204 | -1.45250 | 0.137246 |
| $\theta_w,09$ | -0.94021 | -0.87524 | 0.431023 |
| $\theta_w,12$ | -0.86918 | -1.34994 | 0.791715 |
| $\theta_w,15$ | -0.88081 | -1.52165 | 1.518001 |

Table B-1: Correlation confident of *Vis-Z* pairs for different time windows, different dBZ variables over different radar sample sizes (3x3, 5x5, 7x7, and 9x9). *r* is the correlation coefficient; *SS* is data size.

| Time Window | Z variables | 3x3 | | 5x5 | | 7x7 | | 9x9 | |
|-------------|-------------------------|----------|-----------|----------|-----------|----------|-----------|----------|-----------|
| | | <i>r</i> | <i>SS</i> | <i>r</i> | <i>SS</i> | <i>r</i> | <i>SS</i> | <i>r</i> | <i>SS</i> |
| Time-0 | <i>At</i> | -0.52594 | 304 | -0.52594 | 304 | -0.52594 | 304 | -0.52594 | 304 |
| | <i>Max</i> | -0.55234 | 340 | -0.54962 | 347 | -0.46157 | 358 | -0.4291 | 364 |
| | <i>Min</i> | -0.4975 | 187 | -0.46722 | 29 | -0.49432 | 21 | -0.60617 | 20 |
| | <i>Mean</i> | -0.21415 | 340 | -0.19471 | 347 | -0.16517 | 358 | -0.17455 | 364 |
| | <i>Median</i> | -0.55117 | 308 | -0.53753 | 303 | -0.53358 | 304 | -0.53724 | 300 |
| | <i>Mode</i> | -0.52382 | 256 | -0.47743 | 191 | -0.39143 | 169 | -0.42394 | 178 |
| | <i>MinWithoutZeroN</i> | -0.57948 | 340 | -0.59266 | 347 | -0.57196 | 358 | -0.58183 | 364 |
| | <i>MeanWithoutZeroN</i> | -0.57617 | 340 | -0.59888 | 347 | -0.5716 | 358 | -0.57733 | 364 |
| | <i>AtF</i> | -0.44539 | 187 | -0.42955 | 29 | -0.57839 | 21 | -0.63182 | 20 |
| | <i>MaxF</i> | -0.46871 | 187 | -0.22068 | 29 | -0.4955 | 21 | -0.50799 | 20 |
| | <i>MeanF</i> | -0.49602 | 187 | -0.50842 | 29 | -0.53379 | 21 | -0.59189 | 20 |
| | <i>MedianF</i> | -0.49059 | 187 | -0.50649 | 29 | -0.5371 | 21 | -0.60039 | 20 |
| | <i>ModeF</i> | -0.48393 | 187 | -0.48729 | 29 | -0.55009 | 21 | -0.64043 | 20 |
| time-10 | <i>At</i> | -0.51498 | 303 | -0.51498 | 303 | -0.51498 | 303 | -0.51498 | 303 |
| | <i>Max</i> | -0.54597 | 339 | -0.52335 | 346 | -0.46906 | 357 | -0.44144 | 363 |
| | <i>Min</i> | -0.42151 | 186 | -0.20791 | 28 | -0.39296 | 20 | -0.50669 | 19 |
| | <i>Mean</i> | -0.23602 | 339 | -0.23385 | 346 | -0.19707 | 357 | -0.19267 | 363 |
| | <i>Median</i> | -0.51811 | 307 | -0.51853 | 302 | -0.51699 | 303 | -0.52294 | 299 |
| | <i>Mode</i> | -0.47595 | 255 | -0.35919 | 190 | -0.35001 | 168 | -0.41631 | 177 |
| | <i>MinWithoutZeroN</i> | -0.5618 | 339 | -0.59305 | 346 | -0.57552 | 357 | -0.58618 | 363 |
| | <i>MeanWithoutZeroN</i> | -0.56907 | 339 | -0.59008 | 346 | -0.57618 | 357 | -0.58911 | 363 |
| | <i>AtF</i> | -0.43969 | 186 | -0.23087 | 28 | -0.19227 | 20 | -0.33234 | 19 |
| | <i>MaxF</i> | -0.41544 | 186 | -0.25835 | 28 | -0.46187 | 20 | -0.58672 | 19 |
| | <i>MeanF</i> | -0.43244 | 186 | -0.2657 | 28 | -0.45969 | 20 | -0.54695 | 19 |
| | <i>MedianF</i> | -0.42428 | 186 | -0.23816 | 28 | -0.46894 | 20 | -0.54334 | 19 |
| | <i>ModeF</i> | -0.41638 | 186 | -0.22387 | 28 | -0.42272 | 20 | -0.51651 | 19 |
| Time-20 | <i>At</i> | -0.41871 | 302 | -0.41871 | 302 | -0.41871 | 302 | -0.41871 | 302 |
| | <i>Max</i> | -0.43812 | 338 | -0.40971 | 345 | -0.36541 | 356 | -0.33959 | 362 |
| | <i>Min</i> | -0.30048 | 185 | -0.31844 | 27 | -0.46955 | 19 | -0.51752 | 18 |
| | <i>Mean</i> | -0.17982 | 338 | -0.16153 | 345 | -0.15611 | 356 | -0.14555 | 362 |
| | <i>Median</i> | -0.40691 | 306 | -0.39777 | 301 | -0.4089 | 302 | -0.39289 | 298 |
| | <i>Mode</i> | -0.33853 | 254 | -0.2955 | 189 | -0.26067 | 167 | -0.33713 | 176 |
| | <i>MinWithoutZeroN</i> | -0.42873 | 338 | -0.45377 | 345 | -0.45967 | 356 | -0.46607 | 362 |
| | <i>MeanWithoutZeroN</i> | -0.4482 | 338 | -0.45944 | 345 | -0.45243 | 356 | -0.4664 | 362 |
| | <i>AtF</i> | -0.29734 | 185 | -0.28004 | 27 | -0.4098 | 19 | -0.36176 | 18 |
| | <i>MaxF</i> | -0.32056 | 185 | -0.25823 | 27 | -0.41166 | 19 | -0.40816 | 18 |
| | <i>MeanF</i> | -0.32599 | 185 | -0.29739 | 27 | -0.4669 | 19 | -0.44696 | 18 |
| | <i>MedianF</i> | -0.32287 | 185 | -0.26794 | 27 | -0.46083 | 19 | -0.46448 | 18 |
| | <i>ModeF</i> | -0.31829 | 185 | -0.28698 | 27 | -0.51115 | 19 | -0.46186 | 18 |

Figures

CIR-2421
TEC-177
19 JAN 54

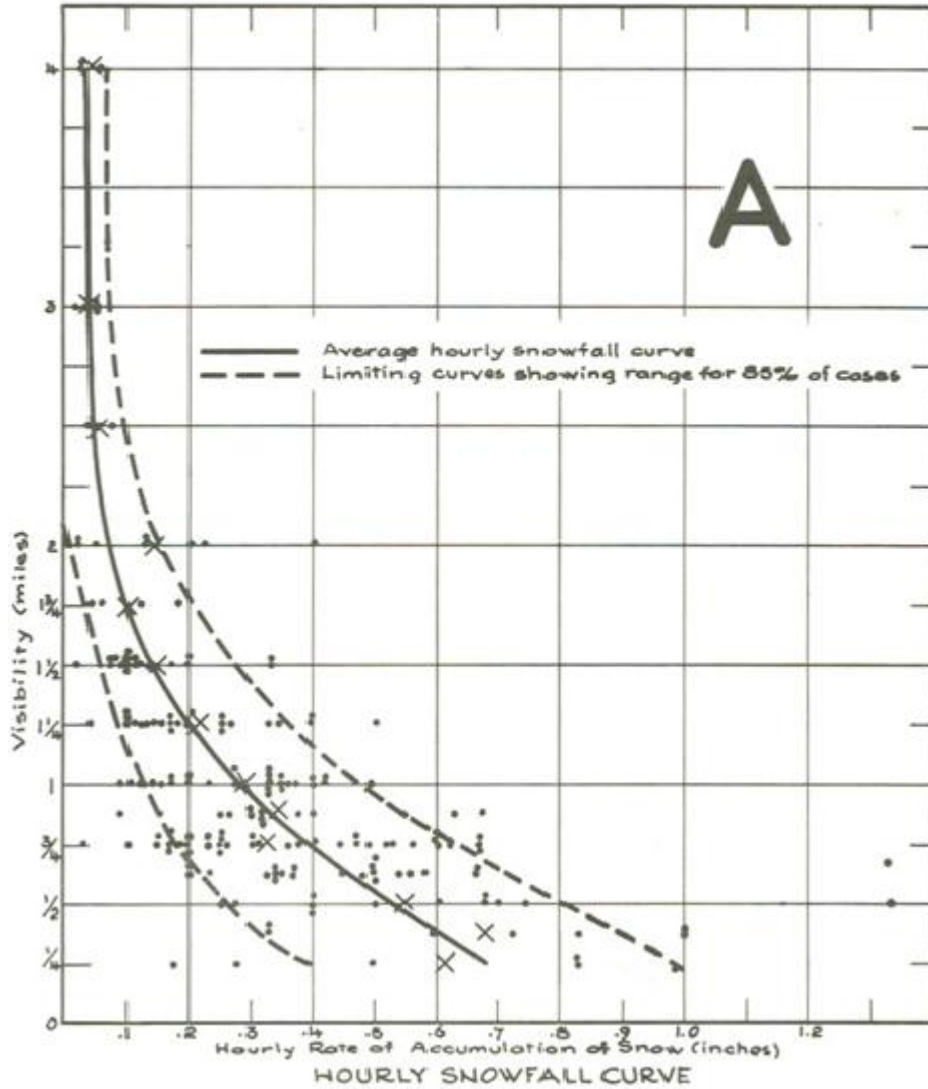


Figure 1.1: Visibility (statute mile) plotted against hourly snowfall (inches) for Canada (taken from Richards 1954). The solid curve gives the best fit to the data. The dashed curves show the limiting cases including 85% of the observations.

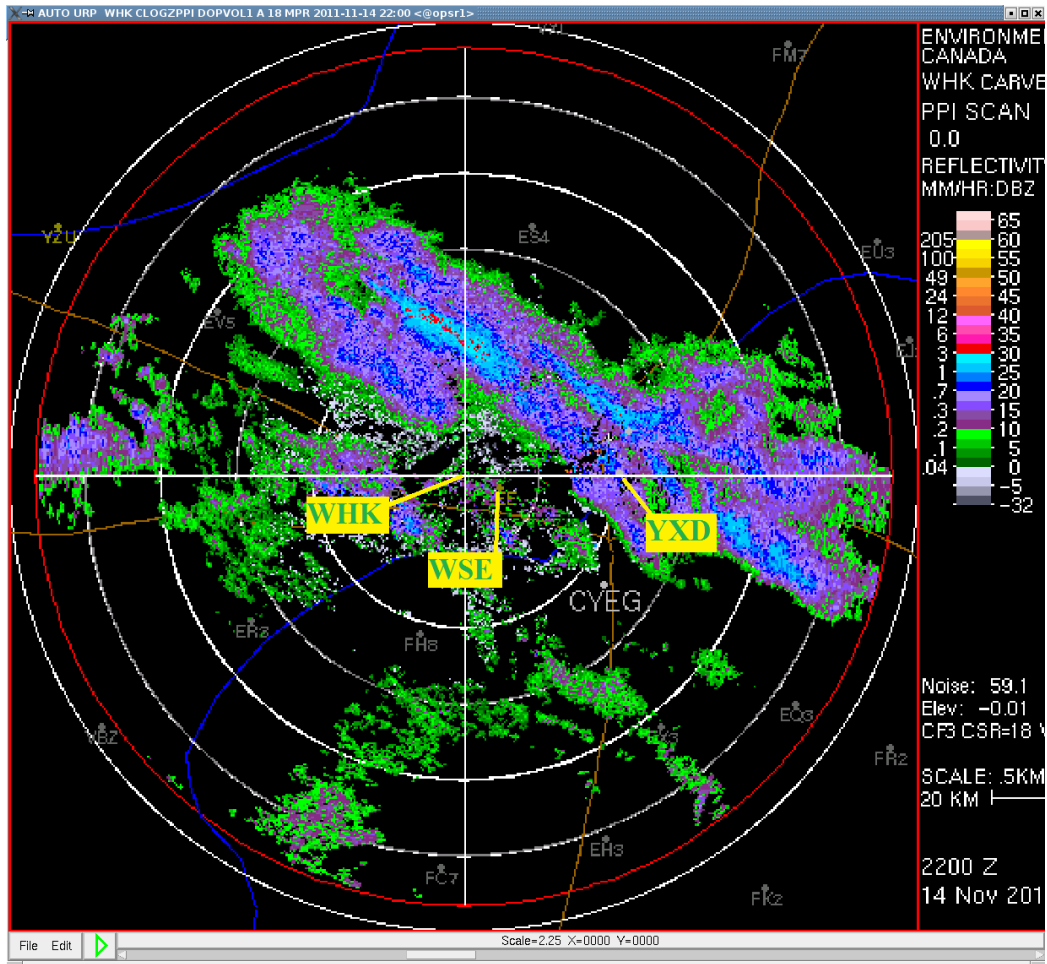
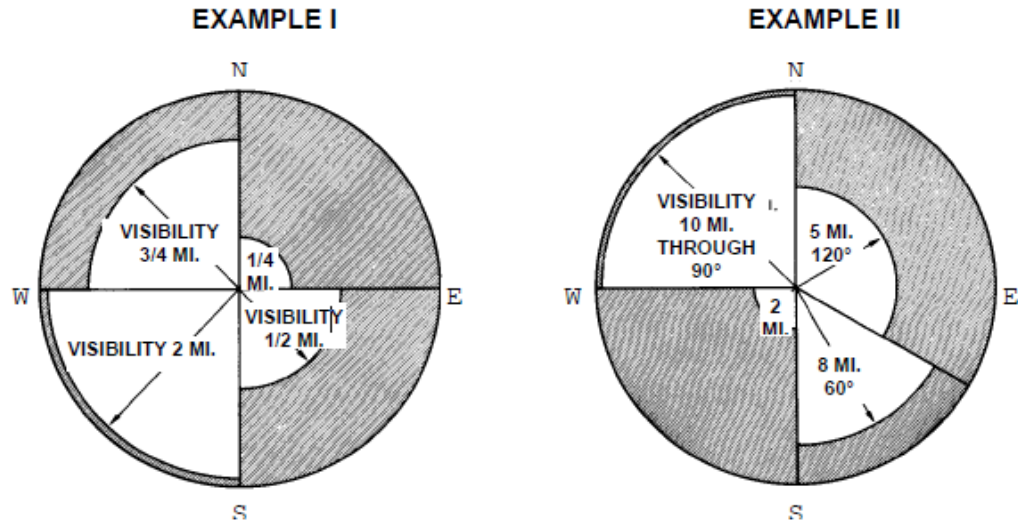


Figure 2.1: A PPI scan of Doppler radar reflectivity. The white concentric rings are 20 km apart. Data source: Environment Canada. Radar name: Carvel (WHK). Elevation angle: 00 degree. Color bar: reflectivity (dBZ) on the right and calculated precipitation rate on the left. Archived time: 2200 UTC, Nov. 14, 2011.

Examples of How to Determine Prevailing Visibility:



NOTE: Point of observation is centre of circle

Figure 2.2: Examples of determining prevailing visibility. The center of the circle is the point of observation. In example I, *Vis* in the 1st quadrant is 1/4mi; *Vis* in the 2nd quadrant 1/2mi; *Vis* in the 3rd quadrant 2mi; *Vis* in the 4th quadrant 3/4mi. In example II, *Vis* in the 1st quadrant is 5mi; *Vis* in the 2nd quadrant 8mi; *Vis* in the 3rd quadrant 2mi; *Vis* in the 4th quadrant 10mi. (Environment Canada, 1977).

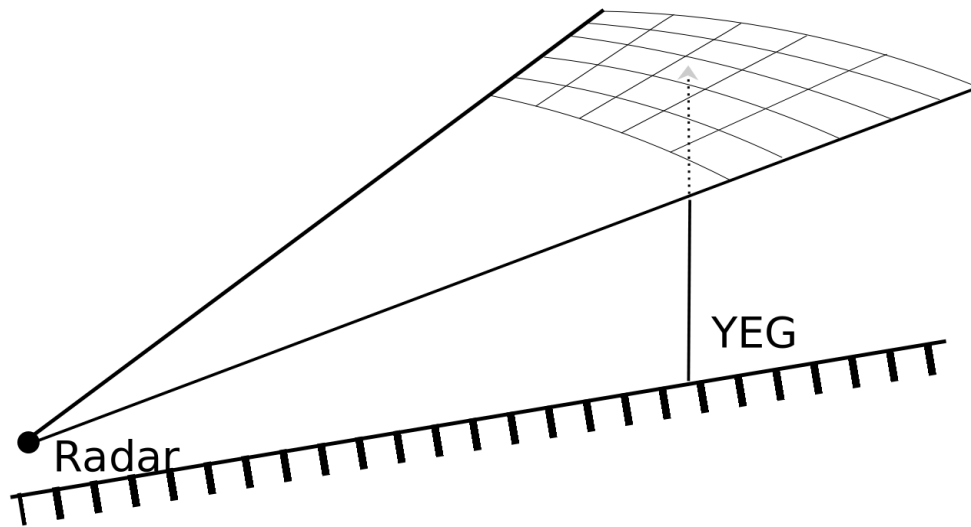


Figure 2.3: Diagram to illustrate a small portion of the radar scan over YEG. The grid centered over YEG denotes the reflectivity sample area in which the median reflectivity value is obtained.

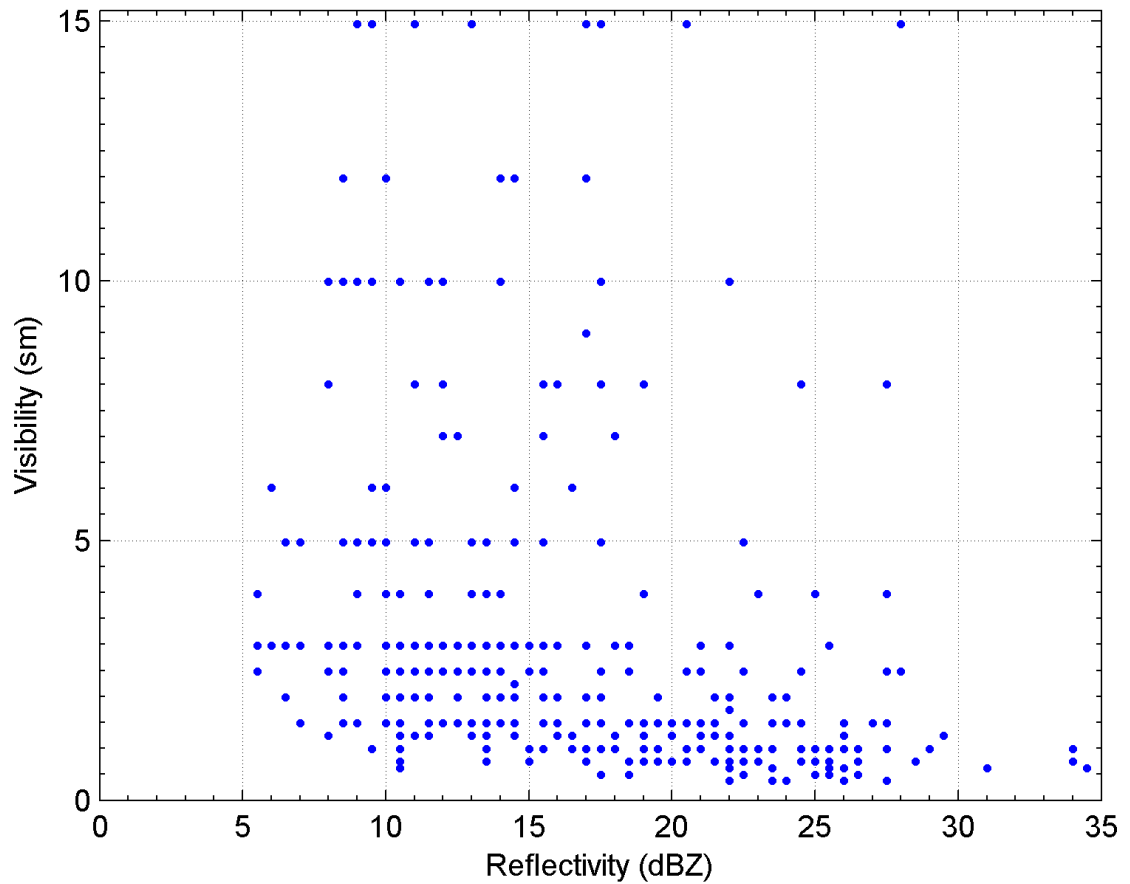


Figure 3.1: Observed Visibility (sm) - Reflectivity (dBZ) data. The visibility is selected when only snow is in the weather group from hourly surface observation from 16 – 23 UTC at YEG. The reflectivity is the median CLOGZ PPI at the elevation angle of 0.0 degree in the sample area of 5 by 5 (near 2.5 km by 2.5 km) centered over YEG. The radar is located at WHK 50 km west of YEG. The scanning frequency of the radar reflectivity is 1 per 10 minutes. The number of data point on the figure is 1017. Both hourly surface observation and radar reflectivity data are from the winter of 2010-11.

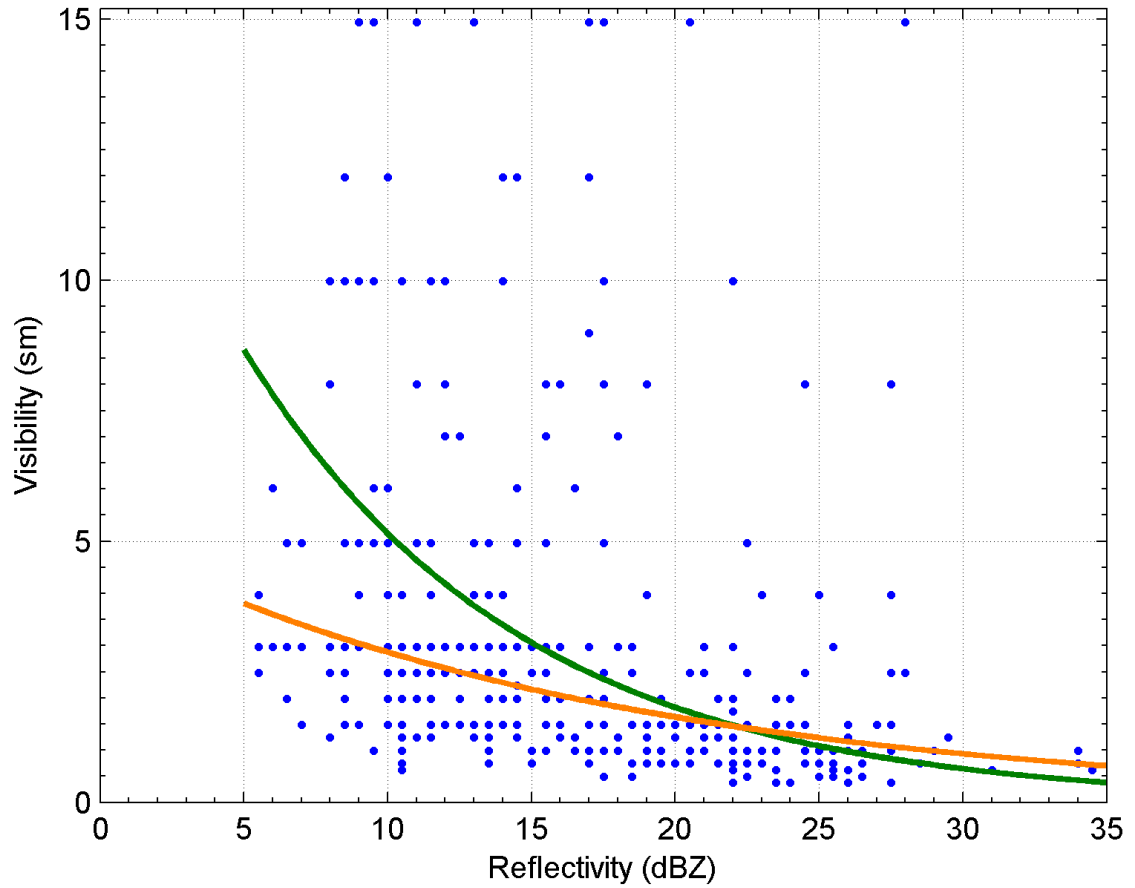


Figure 3.2: The radar based *Vis*-snowfall relationships compared to observed visibility – reflectivity data. For the green line, radar reflectivity is converted into snowfall rate using $Z=1780S^{2.21}$ (Sekhon et al, 1970), and then visibility is calculated using $Vis=2.21S^{-1}$ (Rasmussen et al 1999). For the orange line, radar reflectivity is converted into snowfall rate using $Z=1780S^{2.21}$ (Sekhon et al, 1970), and then visibility is calculated using $\log(\sigma)=0.837+0.542\log(S)$; $Vis=3/\sigma$ (Boudala et al, 2008). The blue dots are the observation data, the same as what is shown in Figure 3.1.

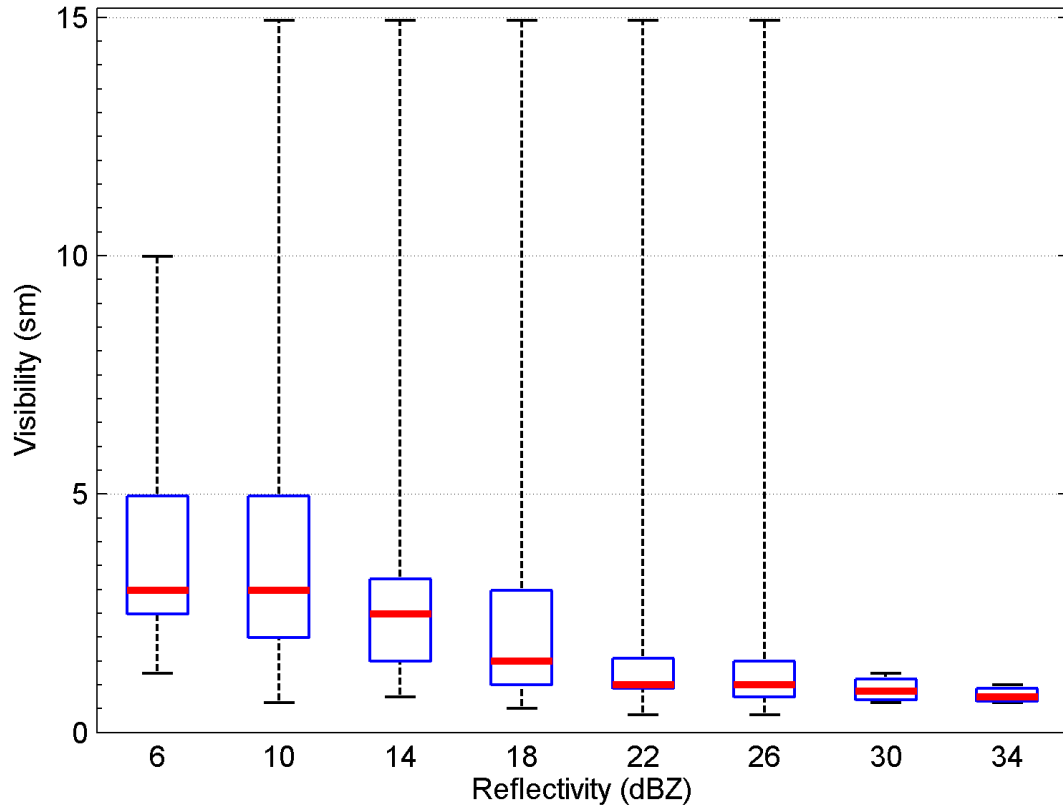


Figure 3.3: Box-and-whisker plots of visibility (sm) for different reflectivity values (dBZ). Each box denotes the 25th-75th percentiles, with a red, heavy solid horizontal bar at the median value. The vertical lines (whiskers) extend to the maximum and minimum values. The reflectivity bins have a width of 4 centered at: 6, 10, 14, 18, 22, 26, 30, and 34 dBZ. The data are the same as the ones on Figure 3.1.

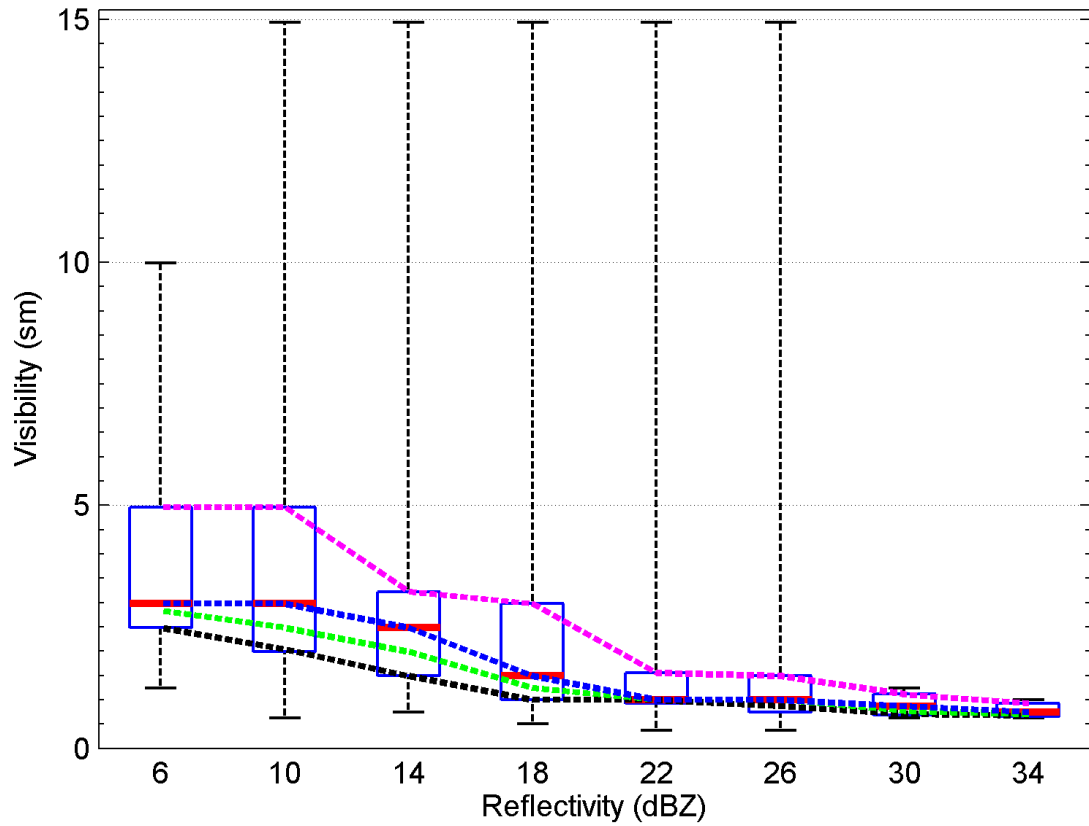


Figure 3.4: Box-and-whisker plots of snow reduced visibility (sm) for different reflectivity values (dBZ) with 30th, 40th, 50th, and 75th percentile curves in black, green, blue, and magenta respectively. The reflectivity groups and data are the same as ones in Figure 3.3. The data are the same as the ones on Figure 3.1.

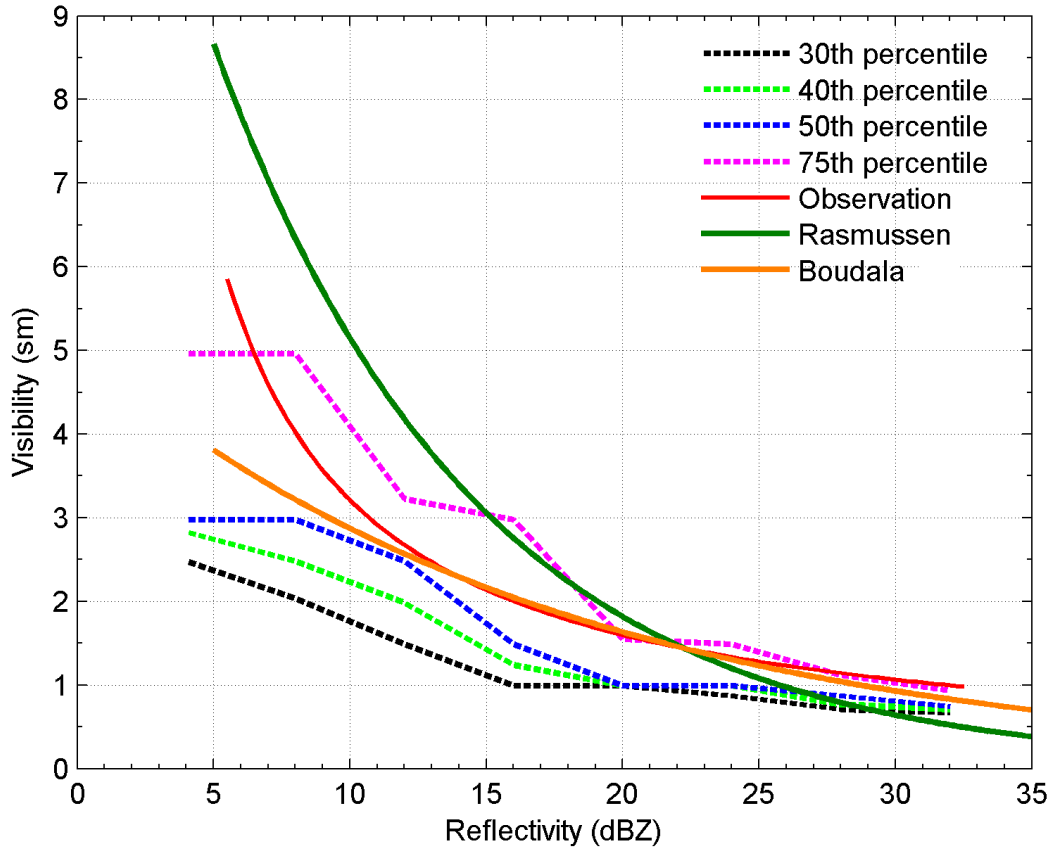


Figure 3.5: Comparison of percentile $Vis - Z$ curves with empirical curves (same as ones in Figure 3.2) suggested by Rasmussen (1998) and Boudala (2010) (same as ones in figure 3.2), and with the $Vis - Z$ regression curves ($Vis = 32.46Z^{-1}$, the correlation coefficient equal to 0.45044, and the root of mean squared error equal to 3.1sm, from the same data in Figure 3.1).

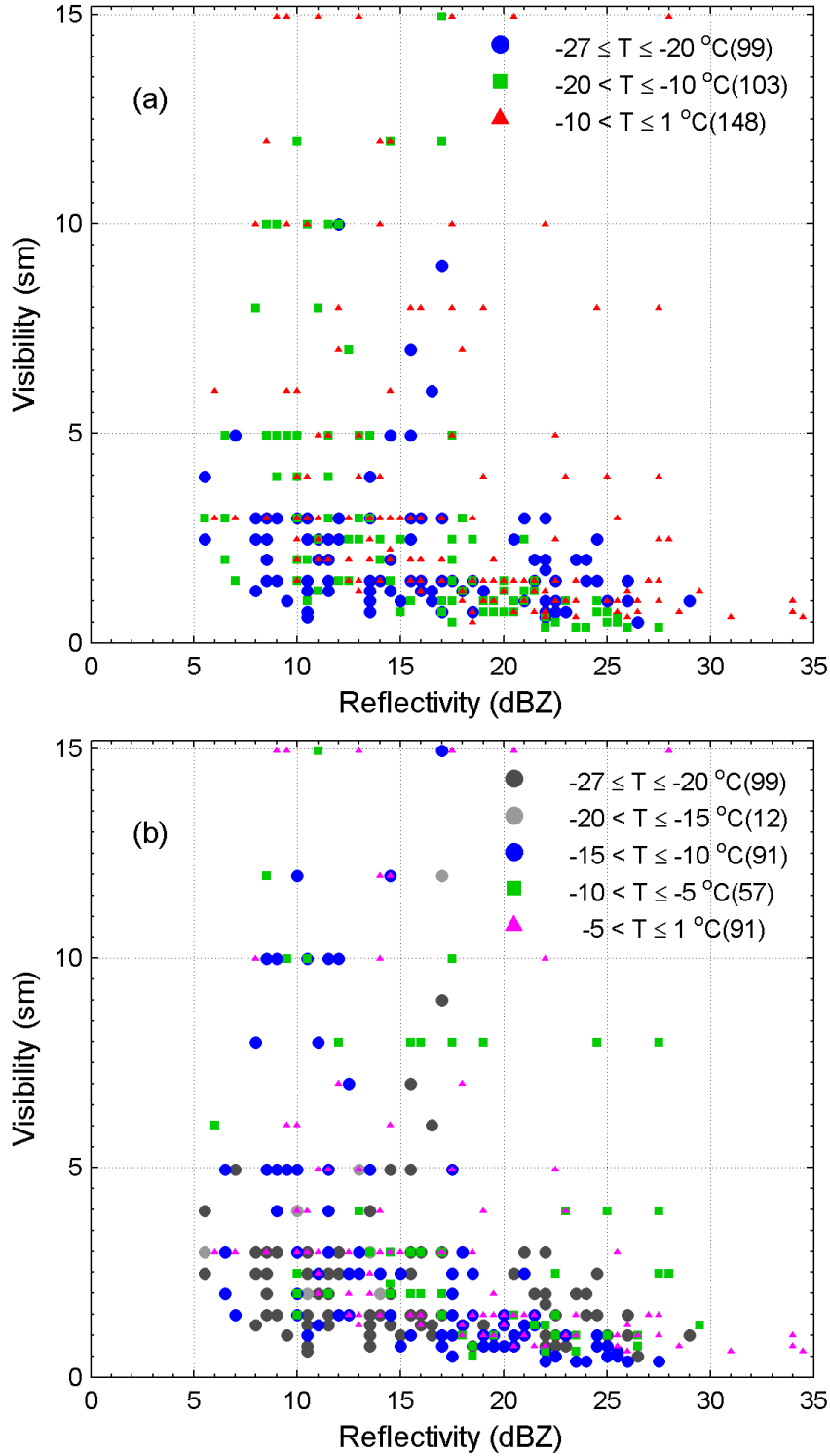


Figure 3.6: Visibility (sm) vs Reflectivity (dBZ) for different surface temperature ranges (a) for detailed temperature ranges, and (b) for coarse temperature ranges. The surface temperature data are from hourly surface observation data in the winter 2010-11. The data are the same as ones in Figure 3.1.

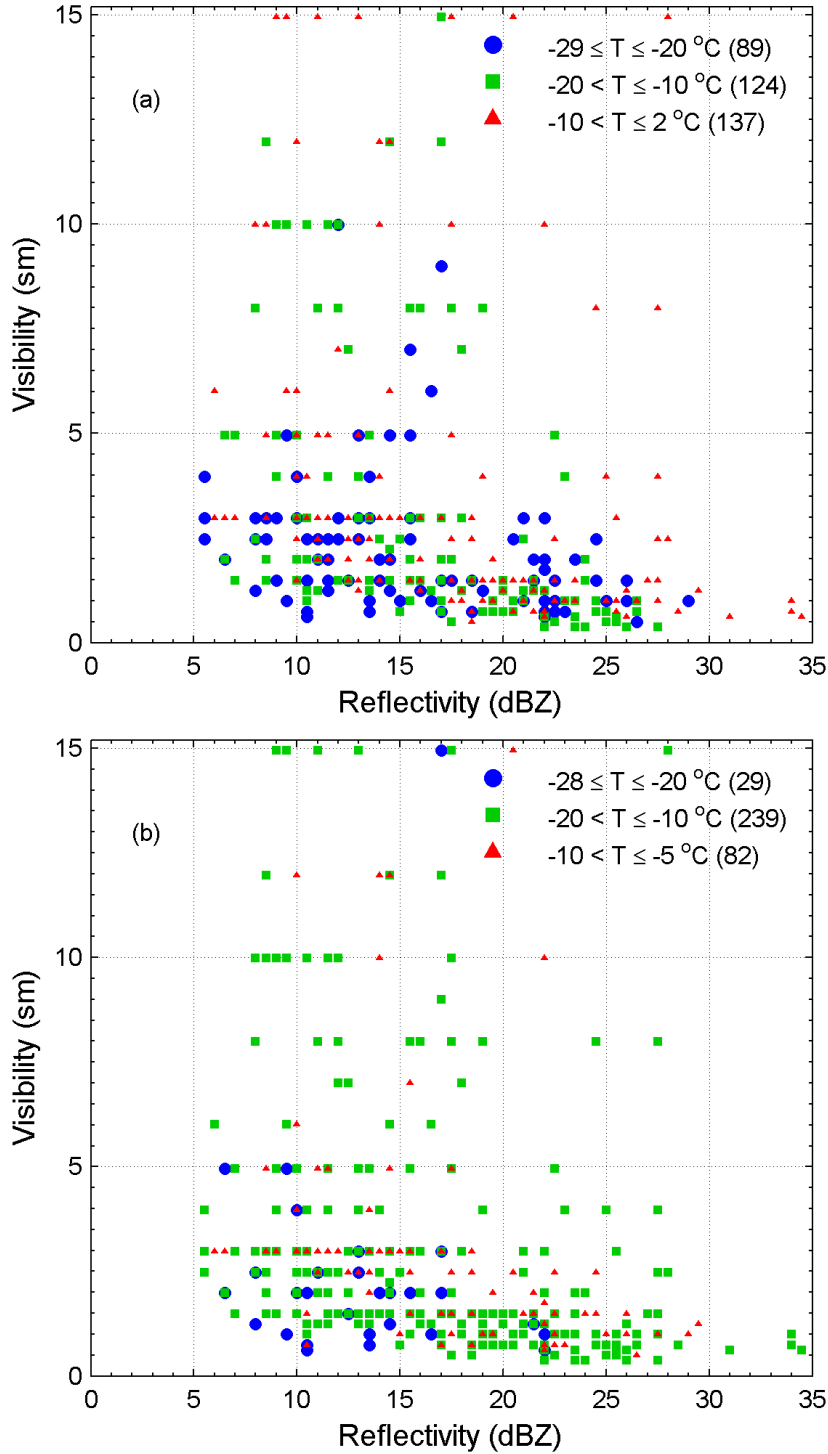


Figure 3.7: Visibility (sm) vs Reflectivity (dBZ) for different upper air temperature ranges (a) at 850 mb, and (b) at 700 mb. The data for visibility and radar reflectivity are the same as ones in Figure 3.1. The upper air temperatures are interpolated into temperature at every 10 minute from the hourly-forecast of vertical temperature made by GEMLAM at 1200 UTC daily.

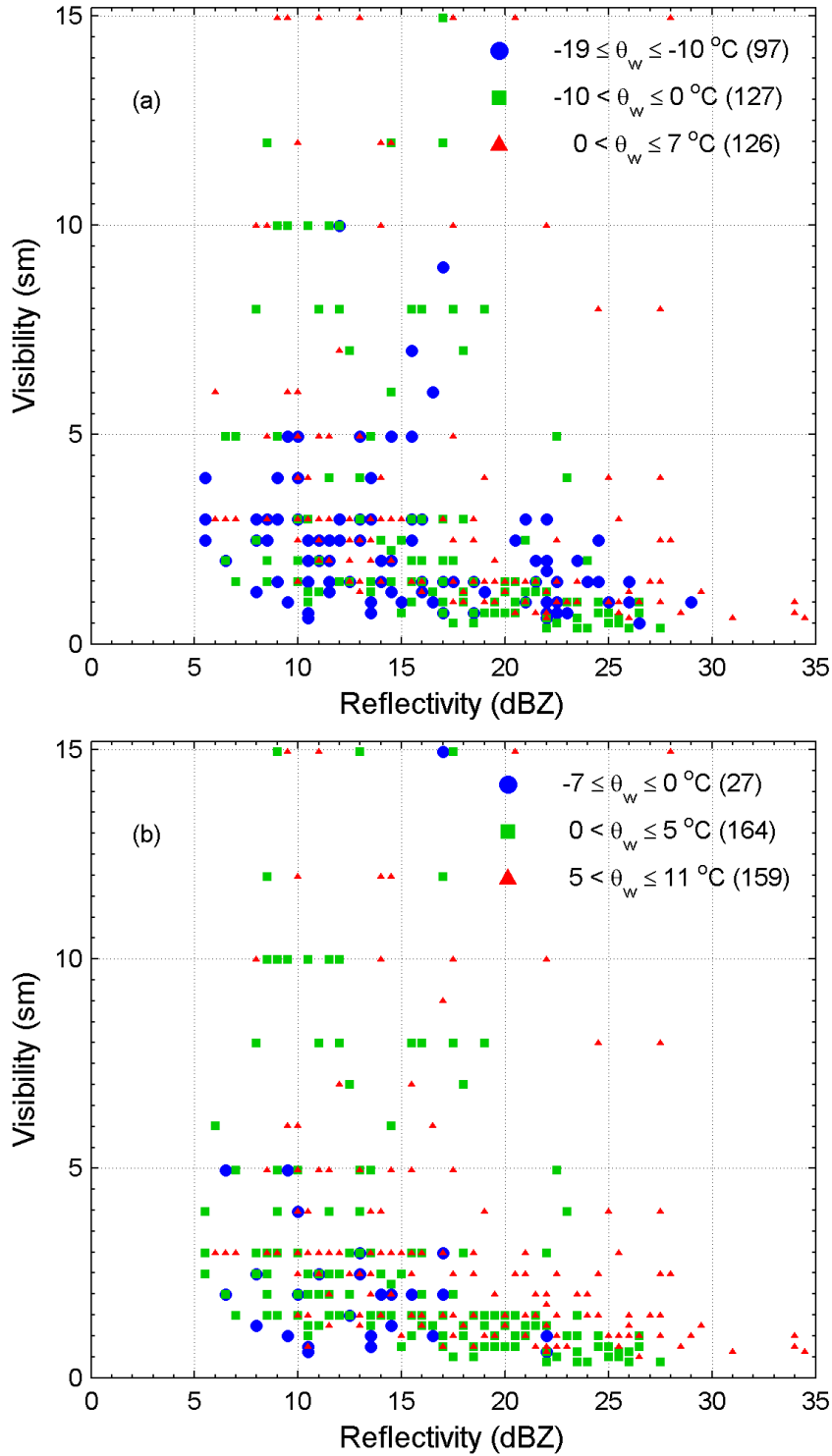


Figure 3.8: visibility (sm) vs Reflectivity (dBZ) for different θ_w ranges at the pressure level of (a) 850 mb, and (b) 700 mb. The observation data for visibility and radar reflectivity are the same as ones in Figure 3.1. The upper air θ_w values are interpolated at every 10 minute from the hourly-forecast of vertical θ_w made by GEMLAM at 1200 UTC daily.

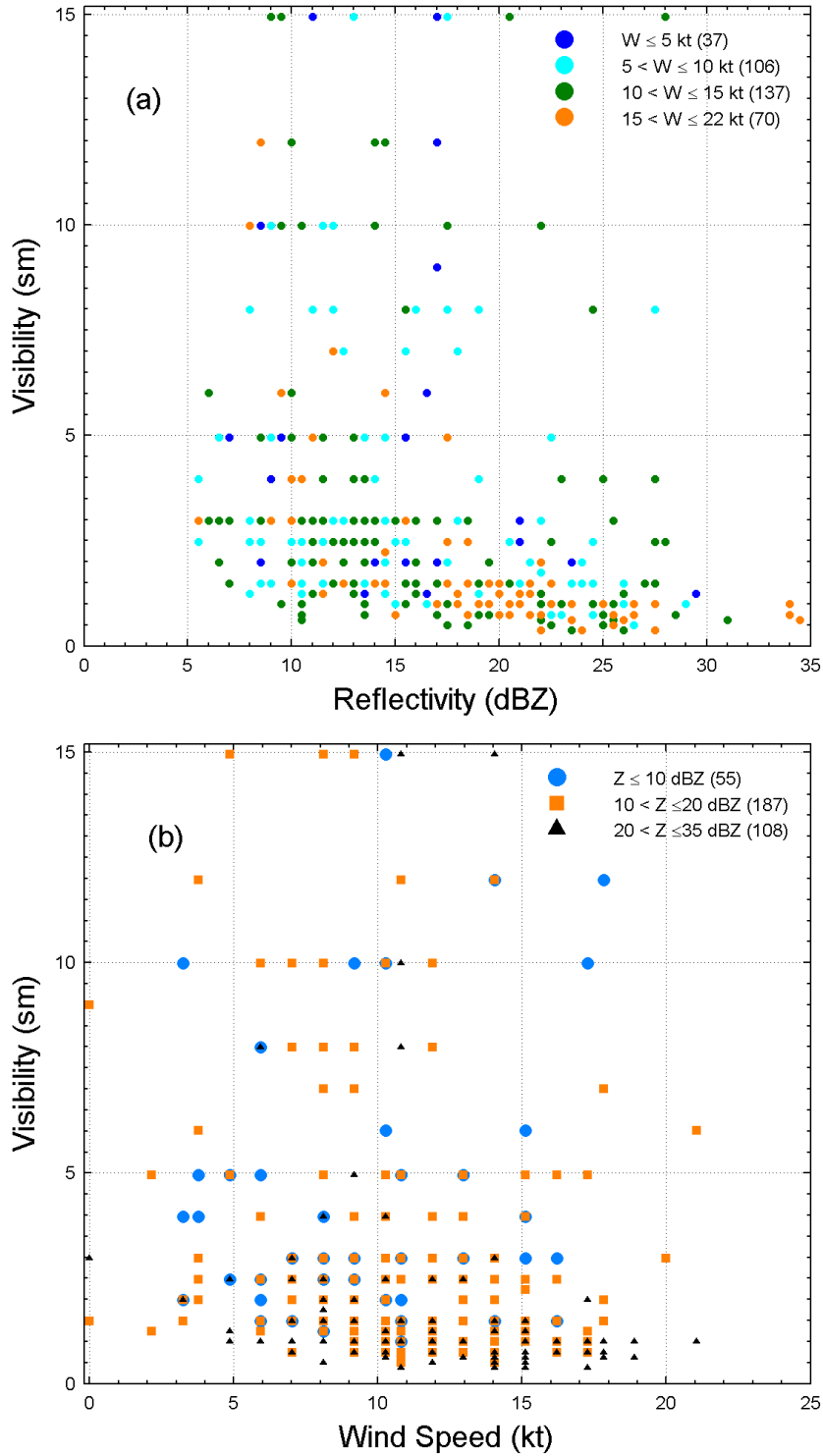


Figure 3.9: The impact of wind on the relationship of visibility (sm) and reflectivity. (a) is Visibility (sm) v.s Reflectivity (dBZ) for different wind (kt) ranges; (b) is Visibility (sm) v.s wind speed (kt) for different reflectivity (dBZ) groups. The data are the same as ones in Figure 3.1.

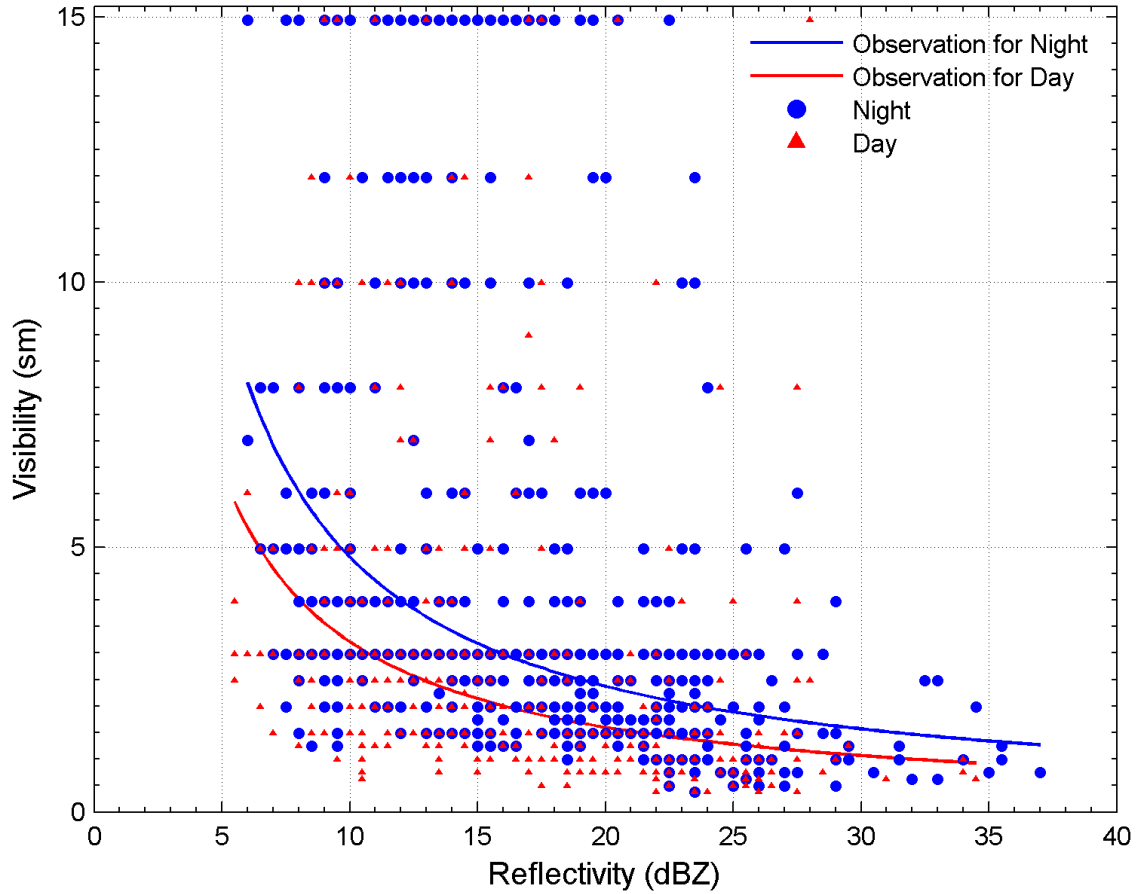


Figure 3.10: Relationship between Snow-reduced visibility (unit: sm from hourly observation at YEG) and Reflectivity (unit: dBZ, observed from the WHK radar with the data collecting frequency of 1 per 10 minutes) the median value in the sample area of 2.5 km by 2.5 km centered over YEG during the winter season of 2010-11 (number of data point: 846). Red triangles denote the data observed from 16 to 23 UTC; the red line demoted the regression equation from the day data: $Vis=32.5Z^{1.0049}$, $r=-0.46$, $rmse=3.1$ sm. The blue dots denote the data observed from 00 – 15 UTC; the blue line denotes the regression equation from the night data: $Vis=50.4Z^{1.02}$, $r=-0.47$, $rmse=3.9$ sm.

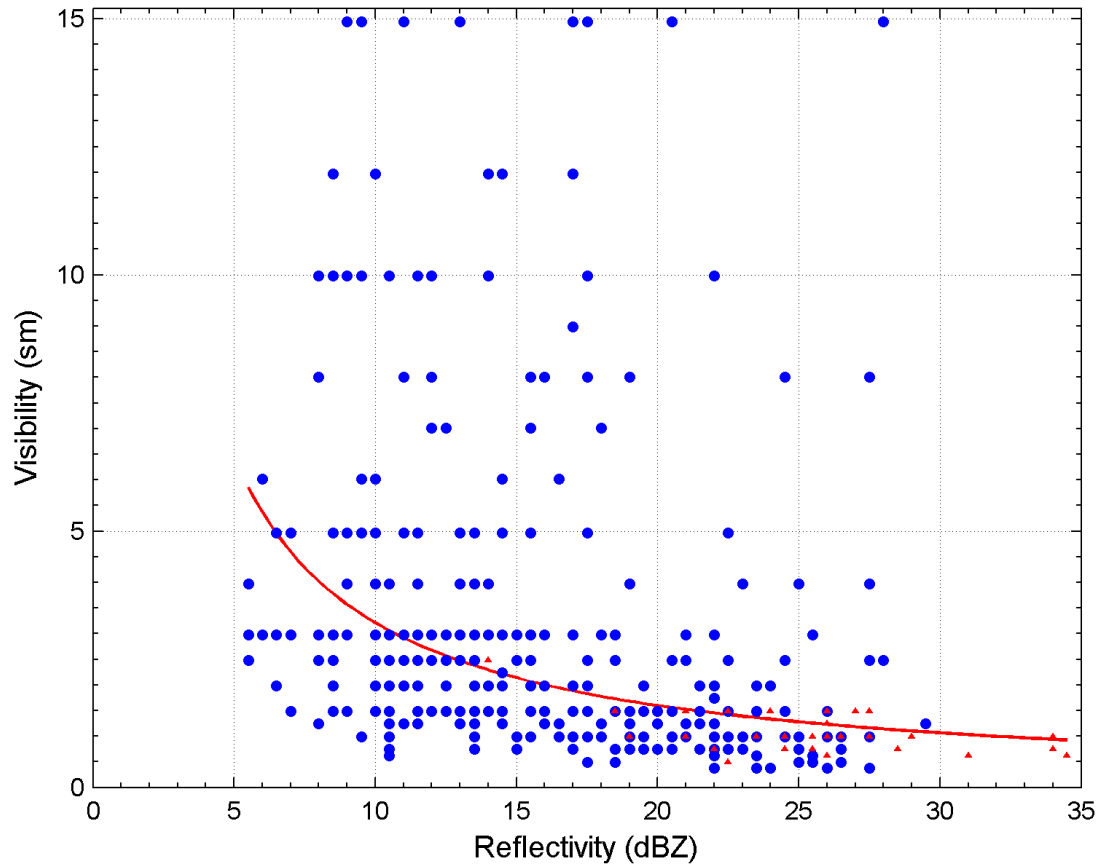


Figure 3.11: Snow-reduced visibility from 16 – 23 UTC (unit: sm from hourly observation at YEG) against Reflectivity (unit: dBZ, observed from the WHK radar with the data collecting frequency of 1 per 10 minutes) the median value in the sample area of 2.5 km by 2.5 km centered over YEG during the winter season of 2010-11 (number of data point: 846). Data with none of Z values equal to -25.5 dBZ in the sample grid pixels are plotted in red triangles (29 data points). Data mixed with Z values equal to -25.5 dBZ in the sample grid pixels are plotted in blue dots. The red line denotes the $Vis - Z$ regression equation based on the data in the blue dots: $Vis = 32.5Z^{-1.0049}$, $r = -0.46$, $rmse = 3.1$ sm.

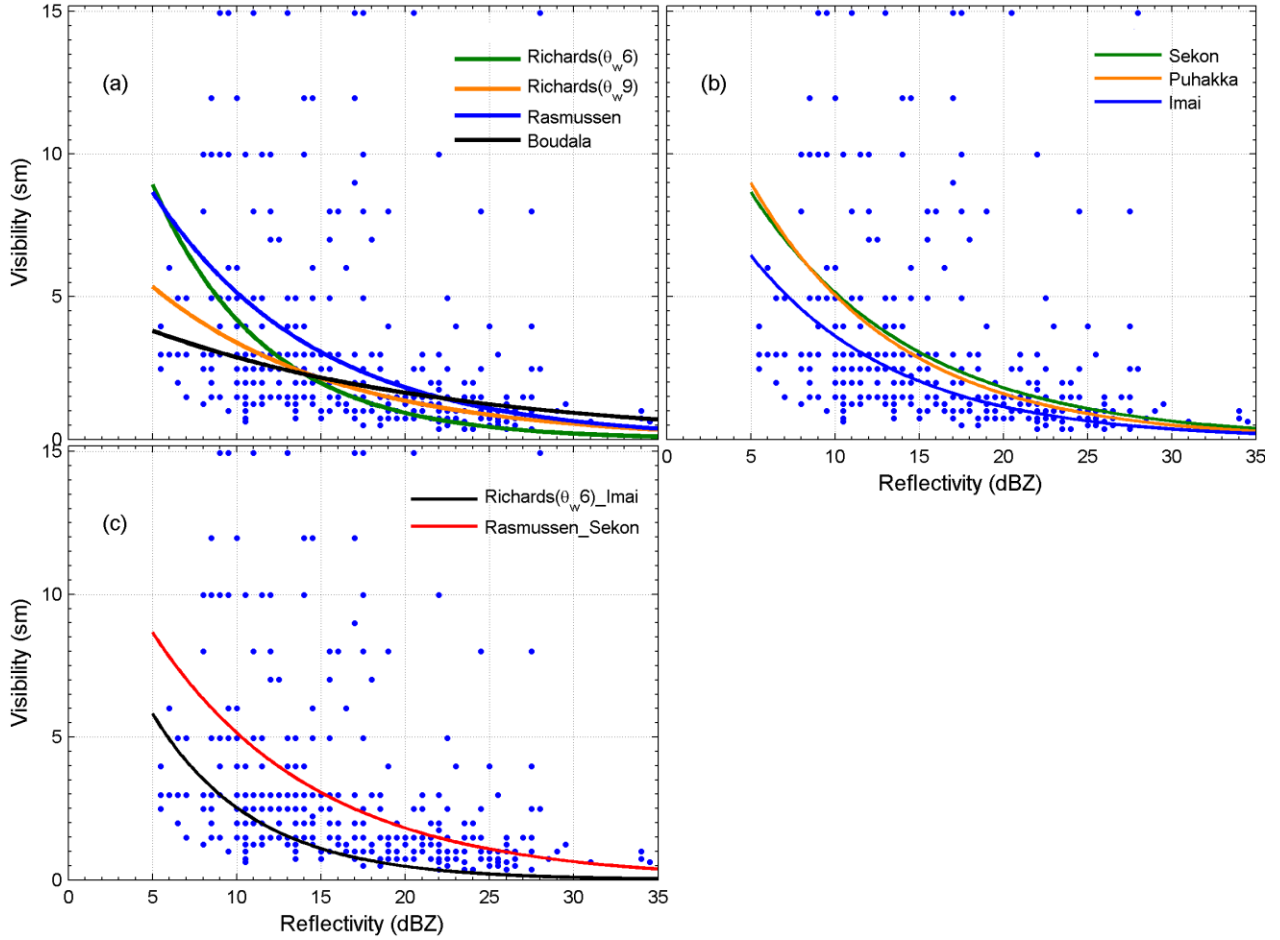


Figure 3.12: Comparisons of different empirical relationships of Vis -radar-based snowfall rate and relationships of Z - S . (a) in green line, Vis calculated by $Vis=0.14S^{-1.55}$ ($\theta_w=6^\circ\text{C}$) (Richards 1954) (See Appendix-2) and S estimated by $Z=1780S^{2.21}$ (Sekhon et al, 1970); in orange line, Vis calculated by $Vis=0.43S^{-0.88}$ ($\theta_w = 9^\circ\text{C}$) (Richards 1954) (See Appendix-2) and S by $Z=1780S^{2.21}$ (Sekhon et al, 1970); in blue line, Vis calculated by $Vis=2.21S^{-1}$ (Rasmussen et al 1999) and S by $Z=1780S^{2.21}$ (Sekhon et al, 1970); in black line, Vis calculated by $\log(\sigma)=0.837+0.542\log(S)$ with $Vis=3/\sigma$ (Boudala et al, 2008) and S by $Z=1780S^{2.21}$ (Sekhon et al, 1970). (b) in green line, Vis calculated by $Vis=2.21S^{-1}$ (Rasmussen et al 1999) and S by $Z=1780S^{2.21}$ (Sekhon et al, 1970); in orange line, Vis is calculated by $Vis=2.21S^{-1}$ (Rasmussen et al 1999) and S by $Z=1050S^2$ Puhakka (1975) ; in blue line, Vis calculated by $Vis=2.21S^{-1}$ (Rasmussen et al 1999) and S by $Z=540S^2$ (Imai, 1960). (c) in black line, Vis is calculated by $Vis=0.14S^{-1.55}$ ($\theta_w=6^\circ\text{C}$) (Richards 1954) and S by $Z=540S^2$ (Imai, 1960); in red line, Vis is calculated by $Vis=2.21S^{-1}$ (Rasmussen et al 1999) and S by $Z=1780S^{2.21}$ (Sekhon et al, 1970). The blue dots are the observation data, the same as what is shown in Figure 3.1.

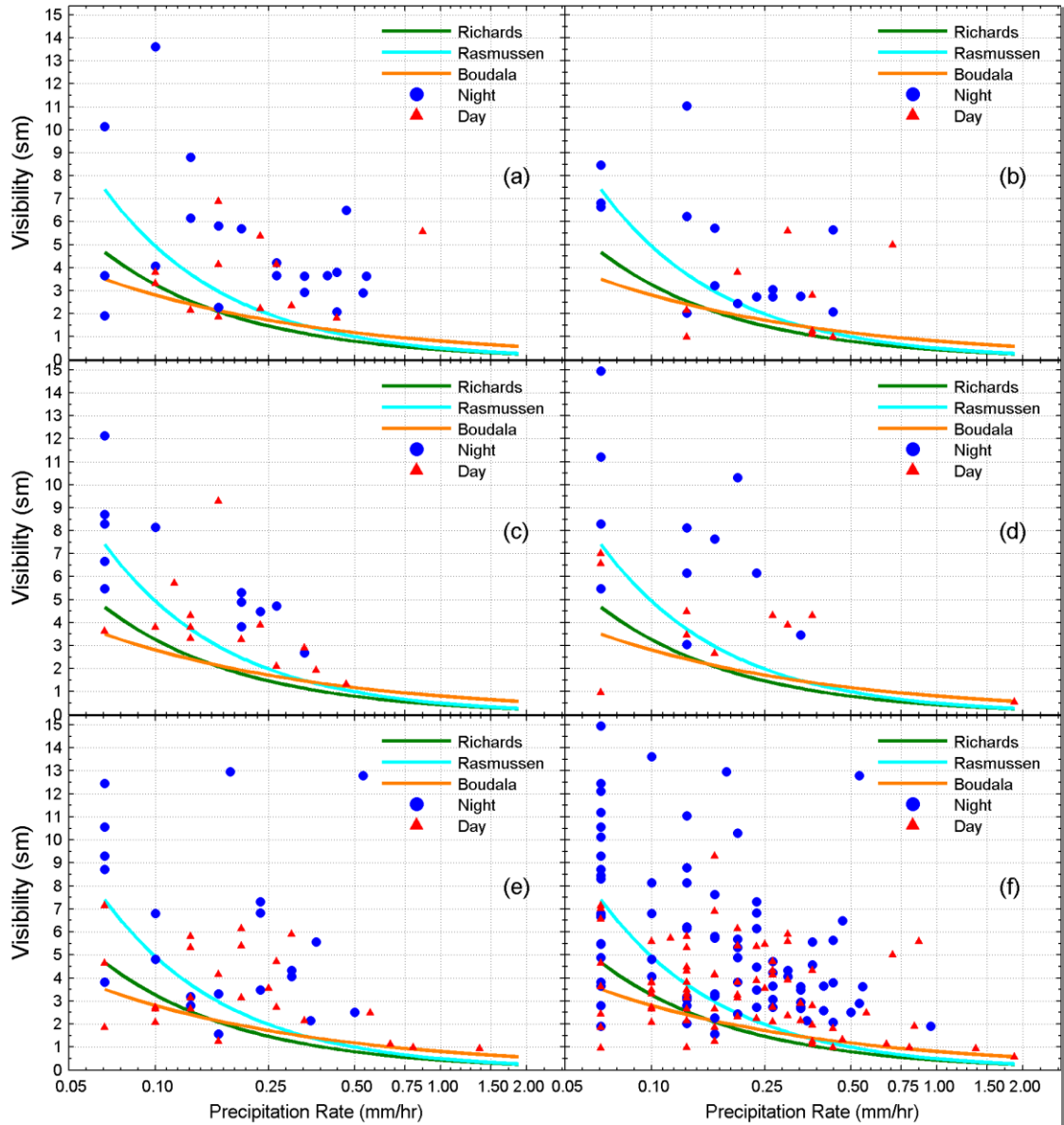


Figure 4.1: The empirical Vis - S relationships compared to the observed Vis - S data (a) for the winter season of 2006-07, (b) for the winter season of 2007-08, (c) for the winter season of 2008-09 (d) for the winter season of 2009-10, (e) for the winter season of 2010-11, and (f) for 5 winter seasons. The visibility data is from hourly observation in the winter seasons from 2006-07 to 2010-11. The precipitation rate data is from 6-hourly precipitation amount data in winter seasons from 2006-07 to 2010-11. The line in green denotes Richards, $Vis=0.43S^{-0.88}$ (Vis in sm, S in mm hr^{-1}); the line in cyan denotes Rasmussen's equation, $Vis=2.21S^{-1}$ (Vis in cm, S in cm/s); the line in black denotes Boudala's equation, $\log(\sigma)=0.837+0.542\log(S)$, $Vis=3/\sigma$ (Vis in km, S in mm hr^{-1}). The red triangles denote the data observed during the day at 18 and 24 UTC with each hour reporting snow in the past 6 hour. The blue dots denote the data observed during the day at 06 and 12 UTC with each hour reporting snow in the past 6 hours.

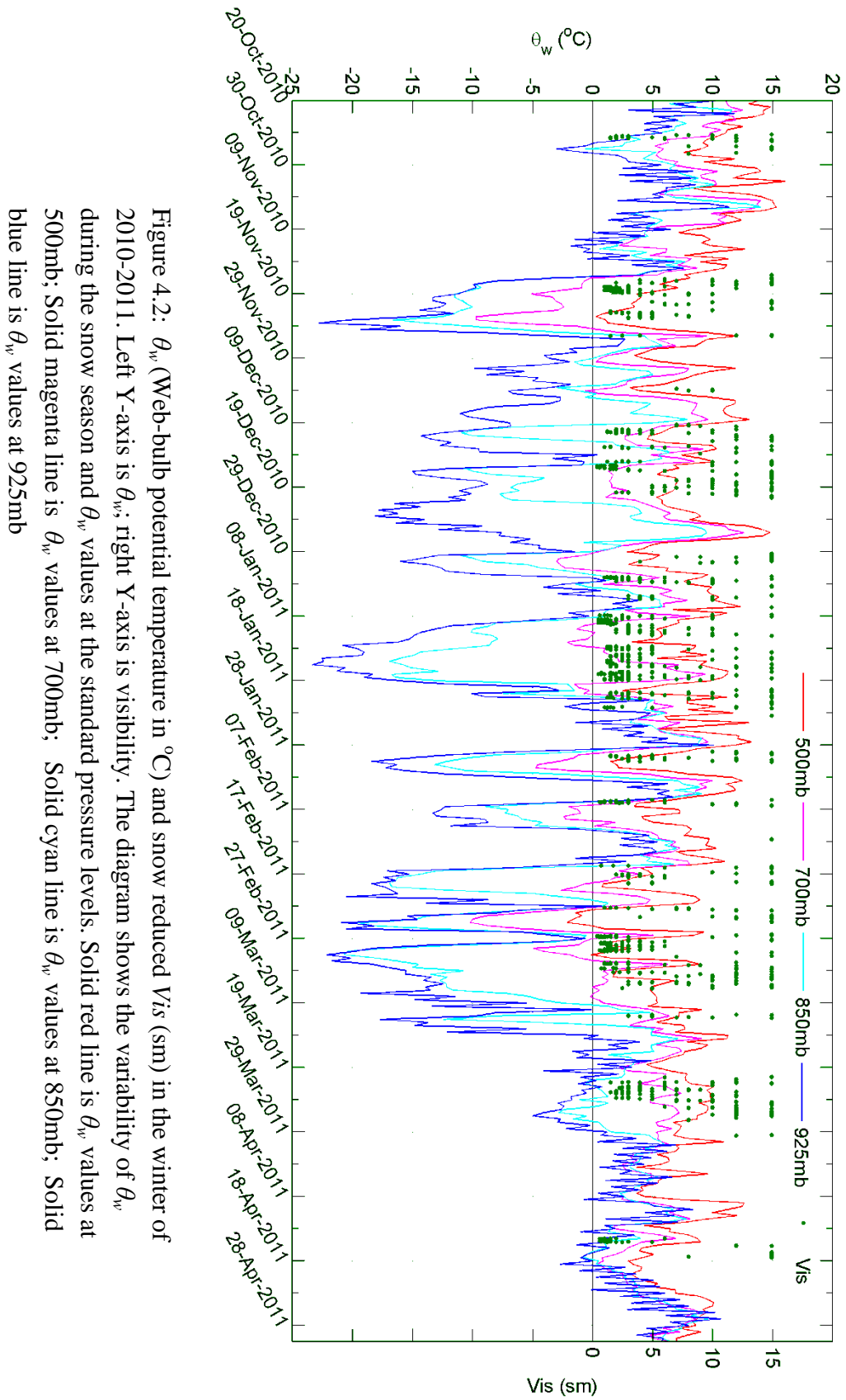


Figure 4.2: θ_w (Web-bulb potential temperature in $^{\circ}\text{C}$) and snow reduced *Vis* (sm) in the winter of 2010-2011. Left Y-axis is θ_w ; right Y-axis is visibility. The diagram shows the variability of θ_w during the snow season and θ_w values at the standard pressure levels. Solid red line is θ_w values at 500mb; Solid magenta line is θ_w values at 700mb; Solid cyan line is θ_w values at 850mb; Solid blue line is θ_w values at 925mb

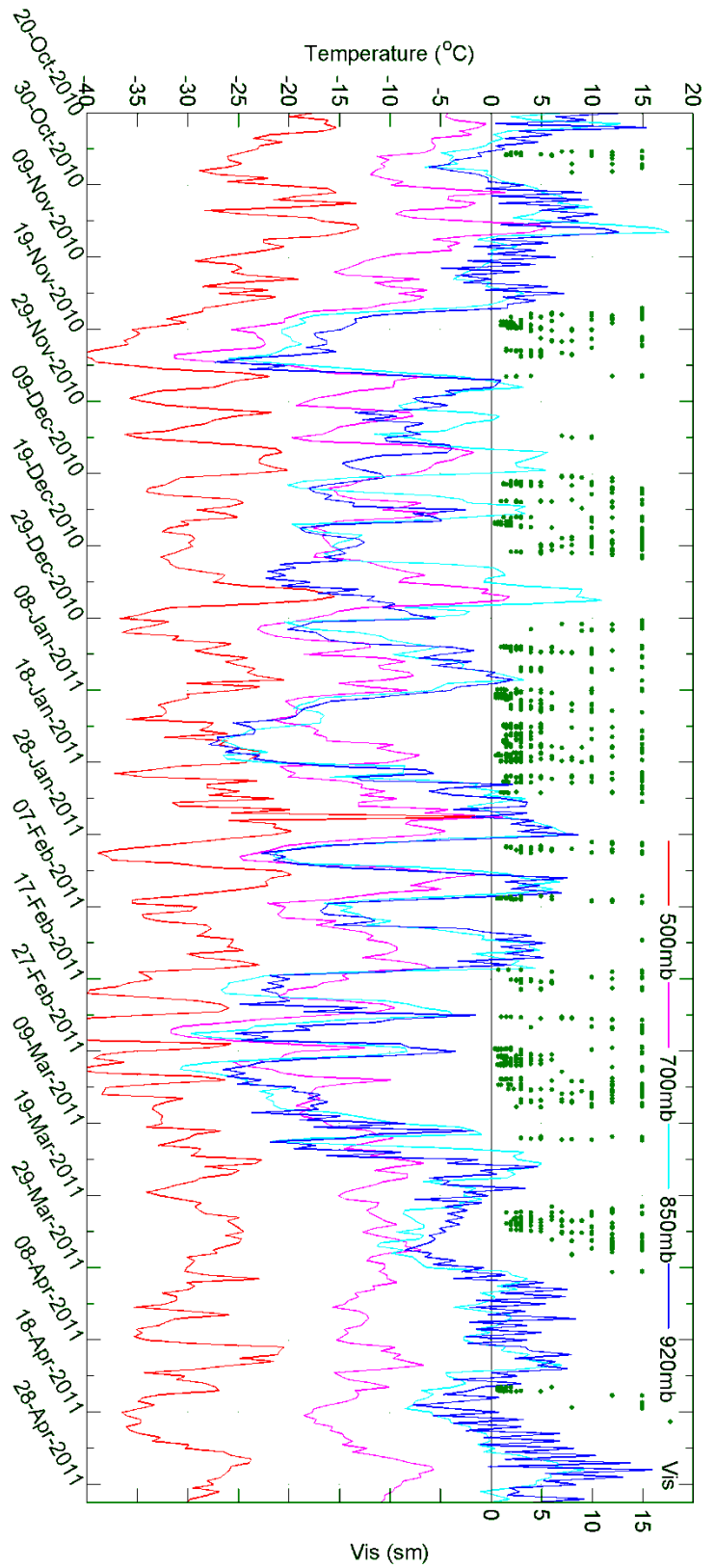


Figure 4.3: Temperature ($^{\circ}\text{C}$) and snow reduced *Vis* (sm) in the winter of 2010-11 (Oct. 2010 to Spr. 2011). The left y-axis is temperature; the right y-axis is *Vis* (sm). The lines of red, magenta, cyan, and blue denote temperature at 500mb, 700mb, 850mb, and 925mb from stony plain soundings. The green dots are *Vis* values when only snow is recorded in the weather group from hourly observation data.

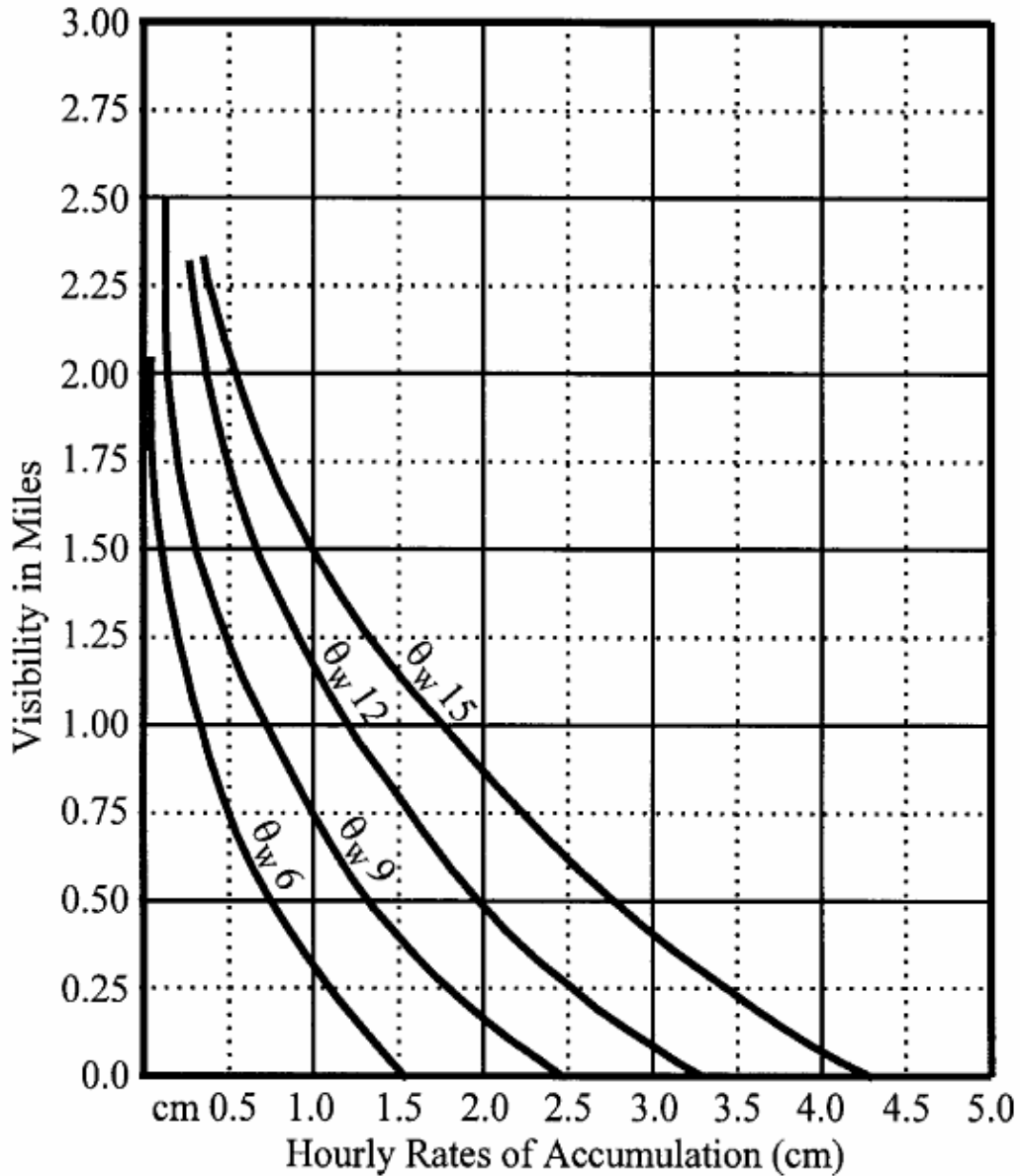


Figure A-1: θ_w curves should be representative of the airmass aloft ahead of the warm front. If airmass snow(circulation flurries) use the θ_w of the airmass. Assume no melting of the snow. Visibility restriction is due entirely to snow. If fog or haze is present, a reduction of as much as 20% would be required. This graph was modified by D. Day, Maritimes Weather Center. Original unknown, but probably from Richards' work. (MOIP, 2001).

Bibliography

- Boudala, F.S., Isaac, G, 2009: Parameterization of visibility in snow: Application in numerical weather prediction models. *J. Geophys. Res.*, **114**, D19202, doi:10.1029/2008JD011130.
- Crozier, C. L., 1986: King Weather Radar operations manual and user's guide, Internal publication, Atmospheric Environment Services, Toronto, 423 pp.
- Environment Canada, 1977, the latest amendment on January 2011: *Manual of Surface Weather Observations (MANOBS)*.. [Available online at http://www.msc-smc.ec.gc.ca/mab/manuals/manobs/enum/pdf/English/titlepg_e.pdf].
- Environment Canada, 1996, the latest amendment on February 11, 2010: *Manual of Standards and Procedures for Aviation Weather Forecasts (MANAIR)*. 6th ed. [Available at <http://www.ec.gc.ca/Publications/default.asp?lang=En&xml=9992D48B-B1B2-4D40-BB9E-234BE164B59E>] retrieve on Mar. 19, 2012
- Environment Canada, 2010: MSC Introductory Weather Radar Course. Topic Scan Strategies and Basic Products. [Available online at <http://courses.comet.ucar.edu/course/view.php?id=33>] retrieved on Mar. 19, 2012
- Hansen, B., 2007: A fuzzy logic-based analog forecasting system for ceiling and visibility. *Wea. Forecasting*, **22**, 1319-1330.
- Imai, I, 1960: Raindrop size distributions and the Z-R relationships. *Proc. Eighth Weather Radar Conf.*, Boston, MA, Amer. Meteor. Soc., 321-326
- Iribarne, J.V., Godson, W. L.,1981: Atmospheric Thermodynamics. 2nd ed. D. Reidel Publishing Company, 259 pp.
- Liou, K., 1980: An Introduction to Atmospheric Radiation. 2ed ed. Academic Press, 392 pp.
- Mahidjiba, A., Donaldson, N., Lapalme, E., 2007: Current Data Format in URP. [Available online at http://collaboration.cmc.ec.gc.ca/cmc/CMOI/produits/samples/radar/vscan/Formats_in_URP.pdf], retrieved on Feb. 15, 2012.
- Marshall, J. S., Palmer, W. McK., 1948: The distribution of raindrops with size. *J. Meteor.* **5**, 165-166.
- Middleton, W. E. K., 1954: *Vision through the Atmosphere*. University of Toronto Press, 250 pp.
- MOIP (Meteorologist Internal Training Program), 2001: Short-range forecasting of cloud, precipitation and restrictions to visibility. [Available at

- http://neige.wul.qc.ec.gc.ca/qww_domaf/TrainingWeb/MOIP_Training_Website/documents/Sujets/Sujet04/mod42a/MOD_042A-2001-10-16.pdf
retrieved on Mar. 19, 2012.
- Muench, H. S. and H. A. Brown, 1977: Measurement of Visibility and Radar Reflectivity During Snowstorms in the AFGL Mesonet. Project 8628, Met Division, Air Force Geophysics Laboratory, Hanscom AFB, Massachusetts. AGFL-TR-77-0148.
- NAV CANADA, 2002: Assessment of Aerodrome Forecast (TAF) Accuracy Improvement Final Report. [Available at http://www.chebucto.ns.ca/Science/AIMET/archive/taf_accuracy.pdf]. Retrieved on March 2, 2012
- Piman, T., Bable, M. S., Das Gupta, A., and Weesakul, S., 2007: Development of a window correlation matching method for improved radar rainfall estimation, *Hydrol. Earth Syst. Sci.*, **11**, 1361-1372.
- Puhakka, T., 1975: On the dependence of the Z–R relation on the temperature in snowfall. Preprints, 16th Conf. on Radar Meteorology, Houston, TX, Amer. Meteor. Soc., 504-507
- Rasmussen, R. M., J. Vivekanandan, J. Cole, J., Myers, B., and Masters, C., 1999: The estimation of snowfall rate using visibility. *J. Appl. Meteor.* **38**, 1542-1563
- Rasmussen, R. M., M. Dixon, F. Hage, S. Knight, J. Vivekanandan, and M. Xu, 2003: Snow Nowcasting Using a real-time correlation of radar reflectivity with snow gauge accumulation. *J. Appl. Meteor.* **42**, 20-36
- Reuter, G,W, and R. Beaubien, 1996: Radar observations of snow formation in a warm pre-frontal snow band. *Atmosphere-Ocean*, **34**, 605-626.
- Richards, 1954: T. L.: An approach to forecasting snowfall amount. TEC 177. 6 pp.
- Rogers, R. R. and M. K. Yau, 1996: *A Short Course in Cloud Physics*. 3rd ed. Butterworth- Heinemann, Burlington, Ma, 290 pp.
- Sauvageot, H. 1992: *Radar Meteorology*. Artech House, Boston, 366 pp.
- Sekhon, R. S., and R. C. Srivastava, 1970: Snow size spectra and radar reflectivity. *J. Atmos. Sci.*, **27**, 299-307.
- Smith, P. L. 1984: Equivalent Radar Reflectivity Factors for Snow and Ice Particles. *Journal of Climate and Applied Meteorology*, **23**, 1258-1260
- Transport Canada, 2011a: Canadian Aviation Regulations (CARs) 2011-2, Part VI – Commercial Air Services, Subpart 2 – Operation and Flight rules, Division III – Pre-flight and Fuel Requirement [Available at

<http://www.tc.gc.ca/eng/civilaviation/regserv/cars/http://www.tc.gc.ca/eng/civilaviation/regserv/cars/part6-602-2436.htm>], retrieved Apr. 4, 2012

Transport Canada, 2011b: Canadian Aviation Regulations (CARs) 2011-2, Part VII – Commercial Air Services, Subpart 5 – Airline Operations, Division III – Flight Operations [Available at <http://www.tc.gc.ca/eng/civilaviation/regserv/cars/part7-705-2146.htm>], retrieved Mar. 20, 2012.

Transport Canada, 2011c: Transport Canada Aeronautical Information Manual (TC AIM), Met – Meteorology, 1.0 General Information [Available at <http://www.tc.gc.ca/eng/civilaviation/publications/tp14371-met-1-0-473.htm>], retrieved Mar. 20, 2012.

Transport Canada, 2011d: Transport Canada Aeronautical Information Manual (TC AIM), RAC – Rules of Air and Air Traffic Service, 3.0 Flight Planning. <http://www.tc.gc.ca/eng/civilaviation/publications/tp14371-rac-3-0-2600.htm>], retrieved Mar. 20, 2012.

Transport Canada, 2011e: Transport Canada Aeronautical Information Manual (TC AIM), RAC – Rules of the Air and Air Traffic Services, 9.0 Instrument Arrival Flight Rules (IFR) – Arrival. [Available at <http://www.tc.gc.ca/eng/civilaviation/publications/tp14371-rac-9-0-2604.htm#9-9>], retrieved Mar. 20, 2012.

Vaisala, 2012: *IRIS Programmer's Manual*, version 8.13.0. Vaisala, Inc.. [Also available at <ftp://ftp.sigmet.com/outgoing/manuals/program/>], retrieved July 20, 2012.

World Meteorological Organization (WMO), 1992: *International Meteorological Vocabulary*. 2nd ed. Secretariat of the World Meteorological Organization. 784 pp.

Appendix A: Re-constructing the *Vis-S* relations of Richards

Richards (1954) suggested that the visibility in snowfall depends on the airmass. The airmass properties can best be quantified in a single parameter: wet bulb potential temperature. Figure A-1 shows 4 curves ($\theta_w 6$, $\theta_w 9$, $\theta_w 12$, and $\theta_w 15$) of Visibility (miles) - Hourly Rates of Accumulation (cm). We searched for *Vis - S* equations that fit to 4 data curves. Values of visibility (*Vis*) and hourly rate of accumulation of snow (*S*) were taken from each curve (Table A-1). In Canada, one centimeter of snow depth is equivalent to 1 millimetre of water equivalent snowfall (Environment Canada, 1977, p. 3-9). So the unit of *S* (water equivalent snowfall) in Table A-1 is mm. We search for a relationship of the form $Vis = aS^m$, where *Vis* is visibility; *S* is snowfall rate; and *a* and *m* are coefficients. The coefficients and correlation coefficients of the best-fitting equations based on the data listed in Table A-1 are listed in Table A-2.

Appendix B: Matching visibility with dBZ variables in different numbers of sample grids with different time window

We had to determine the size of horizontal area for sampling the reflectivity factor data to estimate single Z value to correlate the visibility observed at the Edmonton International Airport (YEG). Also, we had to match the observation time of the radar measurements with the observation time of the visibility. We tested to correlate visibility with other different statistic values of the reflectivity factors observed 0, 10 and 20 minutes before the observation time of visibility in sample grid sizes of 3 by 3, 5 by 5, 7 by 7, and 9 by 9 all centered over the YEG, in order to construct a *Vis-Z* relationship. Piman et al (2007) suggested that one might take adjustments in both time and space to most accurately optimize the relation between the reflectivity factor aloft with surface rainfall. The reflectivity factor variables are named as *A_t* for the reflectivity at the pixel right over YEG, *Max*, *Min*, *Mean*, *Median*, and *Mode*.

Very weak radar returns (the N value would be signed to zero) often occur in the sample data. These zero N value are significantly small than the minimum none zero N values in the sample, and greatly impacted the mean value of the sample and made most minimum values equal to zero except for samples with no zero N values. Therefore, another mean value and minimum values were calculated using the reflectivity factor values after removing these zero N values, named as *MeanWithoutZeroN* for the mean, and *MinWithoutZeroN* as the minimum.

Furthermore, we calculated the maximum value, minimum value, mean value, median value, and mode over the sample size of 3x3, 5x5, 7x7, and 9x9 for cases in which there were no zero N values. These statistics values were named as *A_{tF}* for the reflectivity value at the pixel right over YEG, *MaxF*, *MinF*, *meanF*, *MedianF*, and *ModeF*.

The correlation coefficient (*r*) and the number of data points are listed in Table B-1. It shows no improvement in the relation (indicated by *r*) when

correlating visibility observations with the reflectivity factor observed 10 and 20 minutes before the surface observations. Secondly, there is no improvement in the *Vis-Z* relation when the sample size is greater than 5 by 5 for the *Z* variables obtained from samples containing some zero *N* values. However, the *Vis-Z* relationship slightly was improved as the sample size increases for the *Z* variables obtained from the samples with no zero *N* values. For example, in the time-0 group, for the variable *MedianF*, the correlation coefficient was improved from -0.49059 to -0.60039 as the sample size increases from 3 by 3 to 9 by 9. The dataset size for the samples without any zero in *N* values is much smaller than the dataset size with the samples which could contain zero in *N* values. Comparing among different statistic values, *MinWithoutZeroN* and *MeanWithoutZeroN* are slightly better than the median; however, the median is the best fitting to the prevailing visibility.

In consideration of these factors, we decided to choose the median in the radar sample area of 5 by 5 grids to correlate with the visibility observed at YEG at the same time stamped on the data.